



**PennState**

Vertical Lift Research Center of Excellence  
<http://www.vlrcoe.psu.edu>

# Performance and Design Optimization of the F-Helix eVTOL Concept

**Umberto Saetti**

Graduate Assistant

**Jacob Enciu**

Assistant Research Professor

**Joseph F. Horn**

Professor

Department of Aerospace Engineering

The Pennsylvania State University

University Park, PA 16802

## **Abstract**

The objective of the paper is to study the F-Helix eVTOL concept. This concept modifies the SH-4 Silvercraft light helicopter to use electric propulsion and a propeller-driven rotor. It is intended to compete with rotorcraft in the light-weight class and address future urban air mobility needs. The elimination of shaft driven propulsion is intended to reduce weight and drag in order to accommodate the added weight of batteries for energy storage. Once the configuration of the rotorcraft is established, the design is optimized to produce the least power required while still meeting the structural and physical constraints of its components. Next, a simulation model is developed to assess the rotorcraft performance in hover and forward flight. The payload/range performance is then evaluated for a typical aerial urban transportation mission. The performance of the eVTOL configuration is compared to the SH-4. The flight simulation model is used to assess the dynamic stability of the bare-frame aircraft, along with the stability of the main rotor system. This is done to determine whether additional aerodynamic surfaces such as horizontal and vertical stabilizers are needed to provide acceptable handling qualities to the bare-airframe. Finally, a partial authority Stability and Control Augmentation System (SCAS) is developed to give the aircraft the desired response around the roll, pitch, yaw, and heave axis. The controller also includes a main rotor RPM governor.

## I. INTRODUCTION

### A. Background

The increasing capabilities of batteries will soon justify the transition of light helicopters from fossil fuel to electric power. Numerous concepts of eVTOL rotorcraft were born in recent years with the aim to revolutionize urban air mobility. However, most of these concepts are intended to be fully autonomous, require the development of entirely new platforms, and will have to wait for the development of ad-hoc regulations to become operational. Further, the majority of concepts are based on small distributed propellers with low inertia, which raises questions about their autorotation capabilities. This paper focuses on the study of an eVTOL concept that is intended to compete with existing rotorcraft of the light weight class, and to address the problem of urban air mobility. Some distinguishing features of the concept presented are: it is a piloted rotorcraft, it is based on an existing platform, and it is capable of performing an autorotation.

### B. The Initial F-Helix eVTOL Concept

F-Helix is intended to be a 1-6 seats fly-by-wire electric helicopter that aims to compete with rotorcraft of the same weight class [1]. The concept, as shown in Fig. 1 is based on the idea of reducing initial cost, simplifying maintenance, and being environmentally friendly. The F-Helix concept is powered by two electric ducted fans (eFans) mounted on a “power-mast” connected to the rotor hub. Lift is entirely generated by its two-bladed rotor. The absence of torque exchanged between the fuselage and the main rotor greatly reduces the yaw moment required to trim and control the aircraft, such that small fans can replace the tail rotor and no tail boom is required. The removal of the tail boom reduces weight and drag, and allows the rotor mast height to be reduced. The main transmission is eliminated leading to lower air frame weight and reduced maintenance costs. The weight saved this way is allocated to the battery pack powering the eFans, thus justifying the all-electric approach. Unlike other current eVTOL concepts, F-Helix has a low disk loading and a relatively high rotor inertia, which makes it capable of autorotation. Lastly, F-Helix is based on an existing platform: the Silvercraft SH-4. Table I shows the general characteristics of the SH-4.



(a)



(b)

Fig. 1: (a) Silvercraft SH-4, (b) F-Helix eVTOL initial concept.

### C. Motivation

It is necessary to understand whether the eFan configuration is advantageous with respect to a standard helicopter configuration with an electric motor in place of an internal combustion engine, which will be referred to as an “electric SH-4”. The F-Helix configuration retains the frame and main rotor of the SH-4 (456 lbs) but eliminates the internal combustion engine (Franklin SA-350, 307 lbs), transmission, tail boom, and tail rotor (480 lbs); however it adds a power mast and eFans (estimated weight of 200 lbs), and either a liquid or solid-state Li-Ion

TABLE I: Silvercraft SH-4 characteristics and performance.

Description	Value
Main rotor radius	14.815 ft
Main rotor angular speed	410 RPM
Capacity	1 pilot + 2 passengers
Empty weight	1142 lbs
Maximum takeoff weight	1900 lbs
Power installed	235 shp (derated to 170 shp)
Maximum speed	87 kts
Cruise speed	63 kts
Range	200 mi
Endurance	3 hr
Service ceiling	15090 ft
Rate of climb	1180 ft/min

battery pack are added (1062 lbs, and 665 lbs, respectively). The electric SH-4 eliminates the combustion engine but retains the transmission, tail boom, and tail rotor, and adds an electric engine similar to a Siemens SP55D (100 lbs) used on the Siemens eAircraft [2], and either a liquid or solid state battery pack. Comparing the configurations that use the liquid battery pack, the ratio between the weight of an electric SH-4 and the weight of the F-Helix concept is 1.23. Since the power required ( $P$ ) to hover is proportional to the weight ( $W$ ) of the rotorcraft in the following way:  $P \propto W^{3/2}$ , the ratio of the power required by the two configurations is  $1.23^{3/2} = 1.37$ . This means that the F-Helix concept using a liquid battery pack is competitive with the electric SH-4 if the power losses associated with using the eFans are less than 37%. Comparing the configurations that use the solid-state battery pack, the ratio between the weight of an electric SH-4 and the weight of the F-Helix concept is 1.31. This leads to a ratio of the power required by the two configurations of  $1.31^{3/2} = 1.5$ . This means that the F-Helix concept using a solid-state pack is competitive with the electric SH-4 if the power losses associated with using the eFans are less than 50%. The first part of this study assesses the power required by

the eFans and thus whether the F-Helix concept is justified.

#### D. Objectives

The objective of the paper is to validate and optimize the configuration of the F-Helix eVTOL concept.

- 1) Validate the initial configuration of the F-Helix concept.
- 2) Optimize the design to produce the least power required while still meeting the structural and physical constraints of the various components.
- 3) Assess the performance in hover and forward flight and the payload/range performance for typical missions. Compare performance with performance from the SH-4 helicopter.
- 4) Develop a flight dynamics simulation model.
- 5) Assess the bare-airframe flight dynamics in terms of stability and handling qualities.
- 6) Study the stability of the main rotor system.
- 7) Determine whether additional aerodynamic surfaces such as horizontal and vertical stabilizers are needed to provide acceptable handling qualities.
- 8) Develop and test a partial authority Stability and Control Augmentation System (SCAS) in both batch and piloted simulations. The piloted simulations will be conducted at the newly-built Motion-Base Flight Simulator Lab at Penn State.
- 9) Finalize the design.

## II. DESIGN OPTIMIZATION

### A. Problems with the Initial Design

One concern about the initial design is that the eFans would have to operate under very high centrifugal loads. The eFan centrifugal acceleration is given by:

$$a_c = r_{\text{eFan}} \Omega^2 \quad (1)$$

where  $r_{\text{eFan}}$  is the eFan radial location and  $\Omega$  is the main rotor angular speed. For an eFan located at a radial distance equivalent to the main rotor radius, the centrifugal acceleration would be in the order of thousands of  $g$ 's. Under these conditions the loads on the bearings of fan and motors could possibly create excessive friction and therefore lead to substantial power losses.

This effect can be reduced by lowering the main rotor angular speed and moving the eFans inboard. Lowering the main rotor RPM has the added benefit of reducing noise and improving performance. The added inertia of the eFans will offset the autorotation performance (i.e. can have the same energy index with lower RPM).

The structural integrity of the eFan nacelles is also a matter of concern with the eFans operating under high centrifugal loads. Although ducted fans require less power compared to unducted rotors of the same area to produce the same static thrust, these power benefits tend to decrease with increasing axial flow. Since the eFans are effectively operating in axial flow, the benefits of using ducted fans may not be justified. Further, the eFan nacelles would contribute to the profile drag of the rotor and to the overall frontal drag of the aircraft. It is thus decided to abandon the ducted fans in favour of unducted rotors.

Since the eFans spin in a rotating frame (main rotor), they would produce a large gyroscopic moment in the direction of the power-mast:

$$M_{\text{gyro}} = I_{\text{prop}} \Omega_{\text{eFan}} \Omega \quad (2)$$

where  $I_{\text{prop}}$  is the propeller moment of inertia, and  $\Omega_{\text{eFan}}$  is the eFan angular speed. To counteract the gyroscopic moment, it is decided to mount two counter-rotating coaxial propellers so that the overall gyroscopic moment is zero.

Since there is no torque exchanged between the main rotor and the fuselage, the tail rotor is only used for maneuvering purposes and for providing stability in the yaw axis. Given that the aircraft is symmetric, in trimmed flight the tail rotor has to provide a lower amount of thrust. Since the tail rotor would have to provide thrust in both directions, when the thrust direction changes, the wake rotor inflow has to reverse directions. This would lead to an undesired delay in the control action. For this reason, it is chosen to use two counter-rotating fixed-pitch ducted fans that provide thrust in each direction. These ducted fans will be referred to as “yaw fans”. The amount of thrust in each direction is controlled by the angular speed of the yaw fans. To eliminate time delays due to rotor inflow development, so that the yaw fans are able to produce instantaneous thrust, the yaw fans are chosen to rotate at an idle speed that overall creates zero yaw moment.

Once the configuration of the aircraft is established, the design is optimized to produce the

least power required in hover while still meeting the structural and physical constraints of the various components.

### B. Power Required by eFans in Hover

The first step towards the optimization is the theoretical development of the power required by the eFans in hover. The main rotor power required to hover is calculated by means of momentum theory:

$$P_{MR} = \rho A \Omega^3 R^3 \left( k \frac{C_T^{3/2}}{\sqrt{2}} + \frac{1}{8} \sigma C_{D_0} \right) \quad (3)$$

where:

- $\rho$  is the air density,  $A$  is the rotor disk area,
- $\Omega$  is the rotor angular speed,  $R$  is the rotor radius,
- $k$  is the induced power correction factor,
- $C_T$  thrust coefficient based on the weight of the rotorcraft,
- $\sigma$  is the rotor solidity, and
- $C_{D_0}$  is the section profile drag coefficient.

In addition to the power required by the main rotor, the eFans are required to provide enough power to overcome the aerodynamic drag arising from the power mast. The power dissipated by the aerodynamic drag of the power mast, assuming the same profile power coefficient and chord of main rotor blades, is calculated in a similar fashion to the profile power of a rotor [3]:

$$P_{mast} = \frac{1}{4} \rho \Omega^3 c C_{D_0} r_{eFan}^4 \quad (4)$$

The total power required by each eFan for the rotorcraft to hover is:

$$P_{eFan} = \frac{P_{MR} + P_{mast}}{2} \quad (5)$$

The thrust required by each eFan is:

$$T_{eFan} = \frac{P_{eFan}}{\Omega r_{eFan}} \quad (6)$$

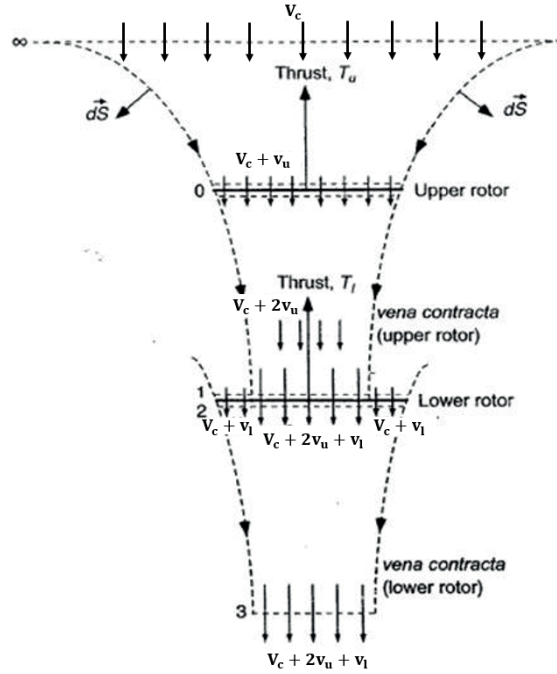


Fig. 2: Flow model assumed for coaxial propellers in axial flow using momentum theory.

Illustration modified from Leishman [3].

### C. Coaxial Propeller in Axial Flow: Momentum Theory

To understand the power required by the eFans electric motors in hover, the equations that describe a ducted fan in an axial flow are derived, thus expanding the theory in [3]. The eFans can be idealized as coaxial propellers operating in a constant axial flow, as shown in Fig. 2. The far upstream velocity relative to the eFan upper rotor, or axial flow velocity, in hover is:

$$V_c = \Omega r_{\text{eFan}} \quad (7)$$

To understand the power required by the electric motors spinning the eFans, the equations that describe a coaxial rotor in an axial flow have to be derived, thus expanding the theory in [3]. Assuming that the thrust produced by each eFan is equally split between the upper and lower rotor, the induced velocity on the upper rotor is:

$$v_u = -\frac{V_c}{2} + \sqrt{\left(\frac{V_c}{2}\right)^2 + \frac{T_{\text{eFan}}}{4\rho A_{\text{eFan}}}} \quad (8)$$

where  $A_{\text{eFan}}$  is the area of each propeller. The upper and lower propellers are assumed to be equal in size and shape. The total power required by the upper rotor is:

$$P_u = k \frac{T_{\text{eFan}}}{2} (V_c + v_u) + \frac{1}{8} \rho N_{B_{\text{eFan}}} \Omega_{\text{eFan}}^3 c_{\text{eFan}} C_{D0_{\text{eFan}}} R_{\text{eFan}}^4 \quad (9)$$

where:

$N_{B_{\text{eFan}}}$  is the number of blades of each eFan propeller,

$c_{\text{eFan}}$  is the eFan blade chord, and

$C_{D0_{\text{eFan}}}$  is the profile drag coefficient of the eFan blades.

The average far upstream velocity of the lower eFan rotor is  $V_c + v_u$ , which leads an induced velocity on the lower rotor of:

$$v_l = -\frac{1}{2}(3v_u + V_c) + \frac{1}{2} \sqrt{(3v_u + V_c)^2 + 8v_u^2 + V_c v_u} \quad (10)$$

The total power required by the lower rotor is:

$$P_l = k \frac{T_{\text{eFan}}}{2} (V_c + v_l) + \frac{1}{8} \rho N_{B_{\text{eFan}}} \Omega_{\text{eFan}}^3 c_{\text{eFan}} C_{D0_{\text{eFan}}} R_{\text{eFan}}^4 \quad (11)$$

The total power required by each eFan electric motor is:

$$P_{\text{motor}} = P_u + P_l; \quad (12)$$

The propulsive efficiency of each eFan is given by:

$$\eta = \frac{T_{\text{eFan}} V_c}{P_{\text{motor}}} \quad (13)$$

#### D. Coaxial Propeller in Axial Flow: Blade Element Momentum Theory (BEMT)

Momentum theory is useful for estimates of the power required but for more detailed information such as the distribution of lift or angle of attack on the rotor blades it is not sufficient. Thus, Blade Element Momentum Theory (BEMT) is developed for the case of coaxial propellers in axial flow. BEMT is a hybrid method that combines basic principles from blade element and momentum theory approaches [3]. Consider the application of the conservation laws to an annulus of a rotor disk. The incremental thrust on the annulus in nondimensional quantities is:

$$dC_T = 2a_w \lambda (\lambda - \lambda_c) r dr \quad (14)$$

where:

$a_w$  is a wake contraction parameter,

$\lambda$  is the total inflow ratio of the eFan, and

$\lambda_c$  is ratio between axial velocity and eFan blade tip speed.

By means of the equivalence between the circulation theory of lift and the momentum theory of lift:

$$dC_T = \frac{\sigma C_{L\alpha}}{2} (\theta r^2 - \lambda r) dr \quad (15)$$

where  $\theta$  is the blade element pitch angle and  $C_{L\alpha}$  is the lift curve slope on the blade profile. Equating the incremental thrust coefficients from the momentum and blade element theories one finds that:

$$\lambda(r, \lambda_c) = \left( \frac{\lambda_c}{2} - \frac{a_w \sigma_{eFan} C_{L\alpha}}{8} \right) + \sqrt{\left( \frac{\lambda_c}{2} - \frac{a_w \sigma_{eFan} C_{L\alpha}}{8} \right)^2 + \frac{a_w \sigma_{eFan} C_{L\alpha} \theta(r) r}{4}} \quad (16)$$

Equation 16 allows for a solution of the inflow as a function of radius and climb velocity for any given blade pitch, blade twist distribution, planform (chord distribution), and airfoil section. Once the inflow is obtained, rotor thrust is found by integration across the rotor disk using:

$$C_T = \int_{r=r_0}^{r=1} dC_T \quad (17)$$

The power coefficient is:

$$C_P = \int_{r=r_0}^{r=1} \lambda dC_T + \frac{\sigma_{eFan}}{2} \int_{r=r_0}^{r=1} \left[ C_{D_0} + d_1 \left( \theta - \frac{\lambda}{r} \right) + d_2 \left( \theta - \frac{\lambda}{r} \right)^2 \right] r^3 dr \quad (18)$$

as for most airfoils the sectional drag coefficient below stall can be approximated by:

$$C_D = C_{D_0} + d_1 \alpha + d_2 \alpha^2 \quad (19)$$

where  $\alpha$  is the angle on attack of each blade element. In this particular application the equations of BEMT are solved numerically. This allows flexibility to incorporate arbitrary variations in twist. The two variations considered are ideal twist:

$$\theta(r) = \frac{\theta_0}{r} \quad (20)$$

and linear twist:

$$\theta(r) = \theta_0 + \theta_{tw}(1 - r) \quad (21)$$

Blade pitch,  $\theta_0$ , is obtained iteratively via bisection method to obtain the required value of thrust coefficient. BEMT is applied separately to the upper and lower eFan rotors with climb ratios of respectively:

$$\lambda_{cu} = \frac{V_c}{\Omega_{eFan} R_{eFan}} \quad (22a)$$

$$\lambda_{cL} = \frac{V_c}{\Omega_{eFan} R_{eFan}} + \lambda_u \quad (22b)$$

The wake contraction parameter  $a_w$  is taken as 0.5 since the eFan propellers are unducted [3].

### E. Yaw Fans Design

Since the yaw rate response can be idealized as a first order system, the required yaw acceleration is given by the ratio of the desired yaw rate and the time constant of the system:

$$\dot{r} = \frac{r_{\max}}{\tau} \quad (23)$$

Values of the desired yaw rate are reported in the large-amplitude heading changes guidelines from ADS-33E-PRF specifications [4]. Assuming that the furthest yaw fan from the CG has negligible thrust at idle angular speed, the yaw acceleration can be related to the yaw fan distance from the CG and to its thrust by the following equation:

$$\dot{r} = \frac{T_{yFan} l_{yFan}}{I_{zz}} \quad (24)$$

where  $I_{zz}$  is the moment of inertia of the aircraft around the vertical ( $z$ ) axis. Since the thrust is proportional to the radius of the yaw fan, an optimization can be carried on to determine the optimal radius and distance from the CG that minimize the yaw fans power while providing the necessary yaw acceleration.

### F. Optimization Results

This section illustrates the results from the optimization of the eFan radial location, radius, and angular speed to minimize the power required from the electric motors spinning the eFans in hovering condition. The variables to be optimized relative to the eFans are the radial location, radius, number of blades and angular speed. For each combination of radial location and radius, the eFan angular speed is chosen to minimize the power required by the eFan while guaranteeing that the angle of attack along the blade span does not exceed 10 deg. This prevents the blade

TABLE II: eFan optimization results.

Parameter	Description	Value
$r_{eFan}$	eFan radial location	8 ft
$R_{eFan}$	eFan radius	1.4 ft
$N_{B_{eFan}}$	eFan number of blades	4 per propeller
$c_{eFan}$	eFan blade chord	0.174 ft
$\Omega_{eFan}$	eFan angular speed	2510 RPM

to operate in stall conditions, with some margin. Figure 3(a) shows how the power required changes with varying eFan radial location and radius. Most notably, the initial configuration with the eFans at a nondimensional radial location of  $r_{eFan} = 1$  would require approximately 105 shp to hover at maximum gross weight. It is suggested that the initial configuration is modified such that eFans are located at  $r_{eFan} = 0.54R$  and have a radius of  $R_{eFan} = 1.4$  ft. This also has the positive side benefit of lowering the centrifugal loads acting on the eFan. For this configuration, the ratio of total power required by eFans electric motors and the power required to spin the main rotor only is 1.23. This indicates that for a constant weight, the F-Helix concept using eFans requires 1.23 times the power that the main rotor only would need to hover (less than a value of 1.37 derived in the Motivation section). Figure 3(b) shows the optimal eFan angular speed with varying eFan radial location and radius. The optimization results are reported in Table II. The corresponding performance in hover at maximum takeoff weight (1900 lbs) and sea level standard day conditions are reported in Table III. Minimum power is approximately 80 shp per eFan, for a total of 160 shp. The required thrust for each eFan 106 lbs. It is concluded that the F-Helix concept using eFans is advantageous, from a power required standpoint, with respect to a standard helicopter configuration that uses an electric engine in place of an internal combustion engine.

The variables to be optimized relative the yaw fans are their radius and location along the aircraft longitudinal axis. The assumed rotor solidity, number of blades, and maximum angular speed are respectively 0.3, 8, and 10000 RPM (approximately 1050 rad/s). Since the yaw fans are

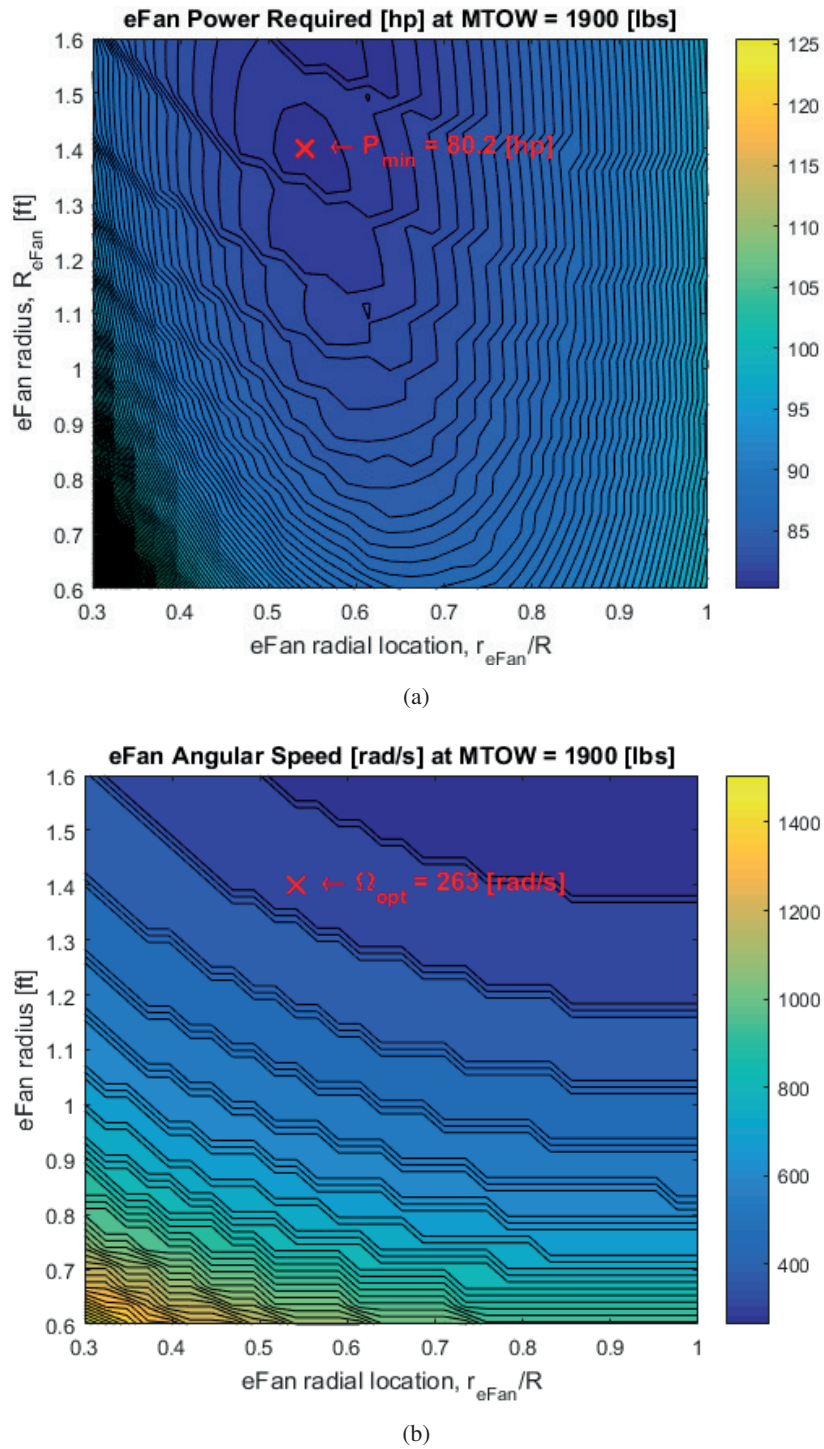


Fig. 3: eFan optimization results: (a) power required and (b) optimal angular speed with varying radial location and radius.

TABLE III: F-Helix performance in hover.

Parameter	Description	Value
$P_{\text{eFan}}$	eFan power required	80 shp
$P_{\text{req}}$	total power required	160 shp
$T_{\text{eFan}}$	eFan thrust	106 lbs
$\eta$	eFan propulsive efficiency	83 %

ducted, the wake contraction factor  $a_w$  is assumed to be 1.25 [3]. For this particular application, the maximum desired yaw rate is chosen to be  $r_{\text{max}} = \pm 9.5$  deg/s. A common value for the time constant for civil rotorcraft is  $\tau = 0.4$  s. The study is approached with BEMT and is effectively a trade-off between distance from the CG (assumed to be located on the main rotor vertical axis) and the yaw fan center. Figure 4 shows the minimum radius to provide the necessary yaw acceleration while guaranteeing that the angle of attack along the blade span does not exceed 10 deg. Although the power required to have the necessary control authority decreases with increasing distance from the CG, increasing distance from the CG leads to a longer and heavier fuselage. For this reason, the distance from the CG of the closest yaw fan is chosen to be 6 ft. The corresponding minimum radius is 0.9 ft. Since the yaw fans amount of thrust is obtained by solely varying the angular speed, the yaw fans operate at constant thrust and power coefficient. The yaw fan thrust and power coefficients are respectively  $2.2 \times 10^{-2}$  and  $3 \times 10^{-3}$ . Peak power required by the yaw fans is about 20 shp. This would be at maximum yaw moment at the start of the yaw rate step. For an assumed idle speed of 500 RPM (approximately 52 rad/s), the power required by each yaw fan is 0.013 shp, which is negligible when compared to the power required by the eFans.

Considering the results from the design optimization, a rendering of the updated F-Helix concept is obtained and showed in Fig. 5.

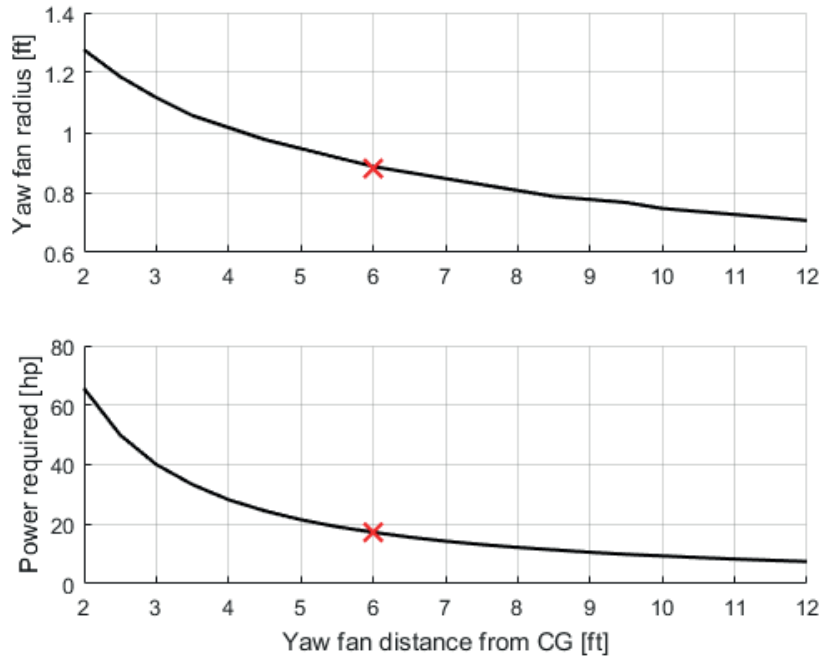


Fig. 4: Yaw fans optimization results.



Fig. 5: F-Helix final concept.

### III. ROTORCRAFT SIMULATION MODEL

A simulation model of the helicopter is required to provide a rigid body six degree of freedom simulation for evaluation of the trim conditions and the basic stability and control characteristics as well as the future design of an automatic flight control system (AFCS) for the eVTOL configuration. The helicopter is modeled as a six degree of freedom rigid body. The model is first developed for a conventional single main rotor helicopter and then modified to account for the specifics of the eVTOL configuration. The simulation model is broken down into modules representing the main and tail rotors, the fuselage, the horizontal stabilizer and the vertical tail. The main and tail rotor models were formulated using a quasi-steady tip path plane model that is developed using analytical integrations of the blade element equations. The Pitt-Peters model [5] is used for the prediction of the dynamic inflow components of the main and tail rotors. The rotor model neglected the lead-lag dynamics as its effect on the rotorcraft trim and primary stability and control characteristics are secondary. The resulting closed form model allowed an efficient calculation of the quasi-steady flapping angles of both rotors and the forces and moments produced by them. Static aerodynamic models were developed for the prediction of the aerodynamic loads produced by the fuselage, horizontal stabilizer, and vertical tail. Simplified wake models were incorporated to simulate the effect of the main and tail rotor wakes on the empennage components. The resulting equations of motion of the rotorcraft can be represented as a nonlinear dynamical system:

$$\dot{\mathbf{x}} = \mathbf{F}(\mathbf{x}, \mathbf{u}) \quad (25)$$

where  $\mathbf{x}$  is the state vector comprised by the rigid body states (inertial velocity and angular rates in body fixed axis, and Euler angles) and the main and tail rotor inflow components:

$$\mathbf{x}^T = \left[ u \ v \ w \ p \ q \ r \ \phi \ \theta \ \psi \ (\lambda_0 \ \lambda_{1c} \ \lambda_{1s})_{MR} \ (\lambda_0 \ \lambda_{1c} \ \lambda_{1s})_{TR} \right] \quad (26)$$

and  $\mathbf{u}$  is the control vector including the lateral and longitudinal pitch command, the collective pitch, and the tail rotor pitch:

$$\mathbf{u}^T = \left[ A_{1c} \ B_{1c} \ \theta_0 \ \theta_{TR} \right] \quad (27)$$

#### A. Conventional Helicopter Model

As production of the Silvercraft SH-4 has ceased in the late 1970s, only very basic engineering data could be tracked down and used. Therefore, the bulk of the data required for the assembly

of the rotorcraft aeromechanical database is collected from two publicly available sources: the specific airworthiness specification for the SH-4 [6] and 1976-1977 edition of “Jane’s all the World’s Aircraft” [7]. The fuselage aerodynamic coefficients were approximated by using the aerodynamic model of the UH60 Black Hawk fuselage of Ref. [8] as a representative conventional fuselage shape. The aerodynamic data is adapted to the SH-4 by using the main rotor radius and disk area as the reference length and area, respectively, for the nondimensional aerodynamic coefficients. The horizontal stabilizer and vertical tail drag, lift and pitch moments were estimated using simple finite wing models. The performance data given in Ref. [7] for the SH-4 were for a Franklin 6A-350-D1B engine derated to 170 shp (127 kW). To allow prediction of the power available and fuel flow data of the SH-4 for performance calculations, the data of an internal combustion engine with a similar available power is used. Therefore the data for a Lycoming HIO-360-B engine with a normal rated maximum power available of 168 shp (125 kW) were utilized for building the power available and fuel flow database. The data is retrieved online from the “O, HO, IO, AIO, HIO, TIO-360 Series Operator’s Manual” [9].

### B. eVTOL Rotorcraft Model

The simulation model for the F-Helix eVTOL configuration is created by modifying the conventional SH-4 model. The tail boom, horizontal stabilizer and vertical tail components were removed from the model and the tail rotor model is replaced by a pair of yaw fans to provide yaw control to the rotorcraft. As described earlier, the idle speed of the yaw fans is assumed to be 500 RPM. However, in order to maintain a net zero yaw moment contribution by the fans at idle speed, the rear fan idle speed is set to 484 RPM to account for its longer arm about the rotorcraft center of gravity. The aerodynamic model of the F-Helix fuselage is modified by reducing the drag, side, and lift forces by 19% to account for the removal of the tail boom and for the smoother aerodynamic shape of the new fuselage in comparison to that of the original SH-4. The reduction factor is determined based on estimates of the expected drag reduction due to the removal of the tail boom was confirmed by the data in Table 6.1 of Ref. [3]. The aerodynamic pitch moment of the new ellipsoid shaped fuselage was evaluated using slender body theory:

$$M = \frac{1}{2} q_{\infty} k V \sin 2\alpha \quad (28)$$

where:

$V$  is the fuselage volume,  
 $k$  is the form factor,  
 $q_\infty$  is the dynamic pressure, and  
 $\alpha$  is the fuselage angle of attack.

This new model replaces the aerodynamic pitch moment coefficient that was used for the SH4. The lateral-directional force and moment coefficients of the SH-4 were not modified for the eVTOL configuration.

The electric power available for performance calculations of the F-Helix is assumed to be independent of ambient conditions. The power available to the eVTOL configuration is assumed to be limited to 200 kW (268 shp). The amount of electric energy available to the rotorcraft is determined by the number and specific energy of the batteries carried by the rotorcraft.

### C. eFan Dynamic Inflow Model

Each eFan is constituted of two counter-rotating coaxial propellers attached to a mast spinning with the main rotor. In case of forward flight, the incident and parallel velocity to each propeller change with rotor azimuth  $\psi_{MR}$ . Consider now a reference eFan. The upper rotor propeller is subject to both axial and tangential flow. The resulting climb and advance ratios for the upper rotor are given by:

$$\lambda_{c_u} = \frac{\Omega r_{eFan} + V_\infty \sin \psi}{\Omega_{eFan} R_{eFan}} \quad (29a)$$

$$\mu_u = \frac{V_\infty \cos \psi}{\Omega_{eFan} R_{eFan}} \quad (29b)$$

where  $V_\infty$  is the absolute speed of the aircraft and  $\psi$  is the azimuth angle of the reference eFan. Assuming that the lower rotor acts in a region where the wake of the upper rotor is fully developed, the incident velocity to the lower rotor is taken as the average between the upper rotor wake velocity, acting on the inner part of the rotor, and the incident velocity to the eFan, acting on the outer part of the rotor. The resulting climb and advance ratios for the lower rotor are:

$$\lambda_{c_L} = \lambda_u + \frac{\Omega r_{eFan} + V_\infty \sin \psi}{\Omega_{eFan} R_{eFan}} \quad (30a)$$

$$\mu_l = \mu_u \quad (30b)$$

where  $\lambda_u$  is the inflow of the upper rotor. Each propeller is modelled with a 1-state inflow model similar to the one described in [5]. The general form of the inflow model is:

$$\dot{\lambda} = -\frac{3}{4}\pi V \lambda + \frac{3}{8}\pi \Omega C_T \quad (31)$$

where:

$\lambda$  is the rotor inflow,

$\Omega$  is the rotor speed,

$C_T$  is the thrust coefficient, and

$V$  is a function of climb ratio, advance ratio, and inflow.  $V$  is given by the following equation:

$$V = \frac{\mu^2 + (\lambda_c + \lambda)(\lambda_c + 2\lambda)}{\sqrt{\mu^2 + (\lambda_c + \lambda)^2}} \quad (32)$$

Since the eFans are collocated opposite to each other, the second eFan will operate at an azimuth angle  $(\psi + \pi)$ . This leads to a 4-state nonlinear system describing the inflow of the upper and lower propellers on each eFan. The thrust coefficients are calculated by means of BEMT. The resulting state and input vector for the F-Helix configuration are:

$$\mathbf{x}^T = \left[ u \ v \ w \ p \ q \ r \ \phi \ \theta \ \psi \ (\lambda_0 \ \lambda_{1c} \ \lambda_{1s})_{\text{MR}} \ \Omega_{\text{MR}} \ \psi_{\text{MR}} \ (\lambda_u \ \lambda_l)_{\text{eFan1}} \ (\lambda_u \ \lambda_l)_{\text{eFan2}} \right] \quad (33)$$

$$\mathbf{u}^T = \left[ B_{1c} \ A_{1c} \ \theta_{\text{TR}} \ \theta_0 \ \Omega_{\text{eFan}} \right] \quad (34)$$

#### IV. PERFORMANCE

The current section presents the results of the trim, point performance and mission performance analyses performed. Trim results were obtained using the dynamic simulation models of the SH-4 and F-Helix. Databases of the power required for hover and cruise were then compiled for point and mission performance calculations. The Lycoming HIO-360-B engine power available and fuel flow database is used for the SH-4. For the F-Helix eVTOL configuration, the maximum power available is assumed constant for all ambient atmospheric conditions as described earlier. The following subsections present the analysis results. Unless specified otherwise all the results presented correspond to sea level standard day conditions (0 ft, 15°C).

### A. Trim Analysis

The trim analysis results are presented for the maximum takeoff weight of 1900 lbs. For the SH-4, the longitudinal center of gravity (CG) is assumed to be positioned halfway between the forward and the aft CG limits. This puts the CG 0.33 ft forward of the main rotor mast. For the F-Helix the longitudinal CG is assumed to be located below the main rotor mast. It is assumed that the rotorcraft could be balanced to this CG position during the detailed design process through proper arrangement of the rotorcraft subsystems and payload distribution.

Figures 6(a)-(f) present the rotorcraft trim attitude angles and control commands as a function of airspeed for straight and level flight. Figure 6(a) shows the fuselage trim pitch angle as a function of airspeed. The results for the SH-4 conventional configuration show that the pitch angle in hover is negative, a result of the CG position being forward of the main rotor mast. Moving from hover into forward flight the pitch angle first increases with airspeed and then decreases. The initial positive gradient of the slope is due to the pitch up moment produced by the horizontal stabilizer. At higher airspeeds the main rotor disk is tilted forward to overcome the fuselage drag and the resulting nose down pitching moment produced by the main rotor counters the nose-up pitch moment of the horizontal stabilizer. In comparison, the hover pitch attitude of the F-Helix is close to zero due to the location of the CG below the main rotor mast. As the F-Helix configuration does not include a horizontal stabilizer, the fuselage pitch angle is monotonically decreasing with airspeed due to the need to tilt the main rotor disk forward to overcome the increasing fuselage drag. The comparison between the two rotorcraft configurations shows that the F-Helix configuration should be more convenient for the passengers due to the lower absolute values of the fuselage trim pitch angles during hover and forward flight. Figure 6(b) compares the fuselage roll trim angle of the two configurations. Unlike the conventional configuration that shows a negative trim angle at all airspeeds the eVTOL configuration has a trim roll angle that is always close to zero. The difference in roll angle between the two configurations is due to the elimination of the tail rotor from the eVTOL configuration. Since the net yaw fan thrust in trimmed flight is essentially zero, the aircraft trims symmetrically, with no lateral tilt of the main rotor required to balance the side force from the tail rotor. Figures 6(c)-(f) present the trim control commands: collective ( $\theta_0$ ), lateral cyclic ( $A_{1c}$ ), longitudinal cyclic ( $B_{1c}$ ) and tail rotor pitch ( $\theta_{TR}$ ), respectively. To allow comparison of yaw control commands between the two

configurations the eVTOL yaw fan RPM commands were converted to equivalent tail rotor pitch commands using a conversion factor of 1124 RPM/deg. This value is derived by assuming that 50% of the tail rotor pitch travel (8.9 deg) corresponds to a maximum yaw fan RPM of 10,000. The collective command for both configurations shown in Fig. 6(c) follows the expected “bell shape” of a conventional rotorcraft. The eVTOL configuration requires a smaller collective pitch than the conventional configuration due to the reduced fuselage drag following the removal of the tail boom, horizontal stabilizer, vertical tail and tail rotor. The lateral cyclic pitch command in Fig. 6(d) (positive to the right) reflects the increasing right tilt of the main rotor disk with airspeed that has to be countered by a left cyclic pitch command. The longitudinal cyclic pitch command (Fig. 6(e)), follows the trend explained earlier for the fuselage trim pitch angle. The negative apparent longitudinal stability of the SH-4 at airspeeds between 30 KTAS and 39 KTAS is a result of the main rotor wake effect on the horizontal stabilizer. In comparison, the F-Helix shows apparent positive stick stability throughout the flight speed envelope. Finally, figure 6(f) that shows the tail rotor pitch command as a function of airspeed demonstrates the advantage of eliminating the tail rotor in the eVTOL configuration. As the power to drive the main rotor shaft is transmitted directly through the eFans, no torque is transmitted to the fuselage. Therefore, the power required to turn the tail rotor in a conventional rotorcraft is saved and only a small amount of yaw control is required to balance the contribution of the fuselage aerodynamic loads to the yaw moment about the rotorcraft CG.

### *B. Point Performance*

Hover out of ground effect (OGE) and forward flight performance were calculated for both configurations and are compared in the current subsection. The objective of the comparison is to point out the key differences in point performance between the conventional rotorcraft and the eVTOL configuration. The torques required for hover and forward flight were first calculated using the simulation models for both configurations. The simulation model for the SH-4 is then tuned to match the performance data of Ref. [7]. Specifically, the maximum hover weight is matched by tuning the rotor blades profile drag coefficient ( $C_{D_0}$ ) and induced power factor ( $k$ ) and the “economic cruise speed” (speed for maximum range) is matched by adjusting the horizontal equivalent flat plate area (EFPA) of the fuselage. For the calculation of the F-Helix performance the same values for main rotor parameters were used, and the fuselage drag is

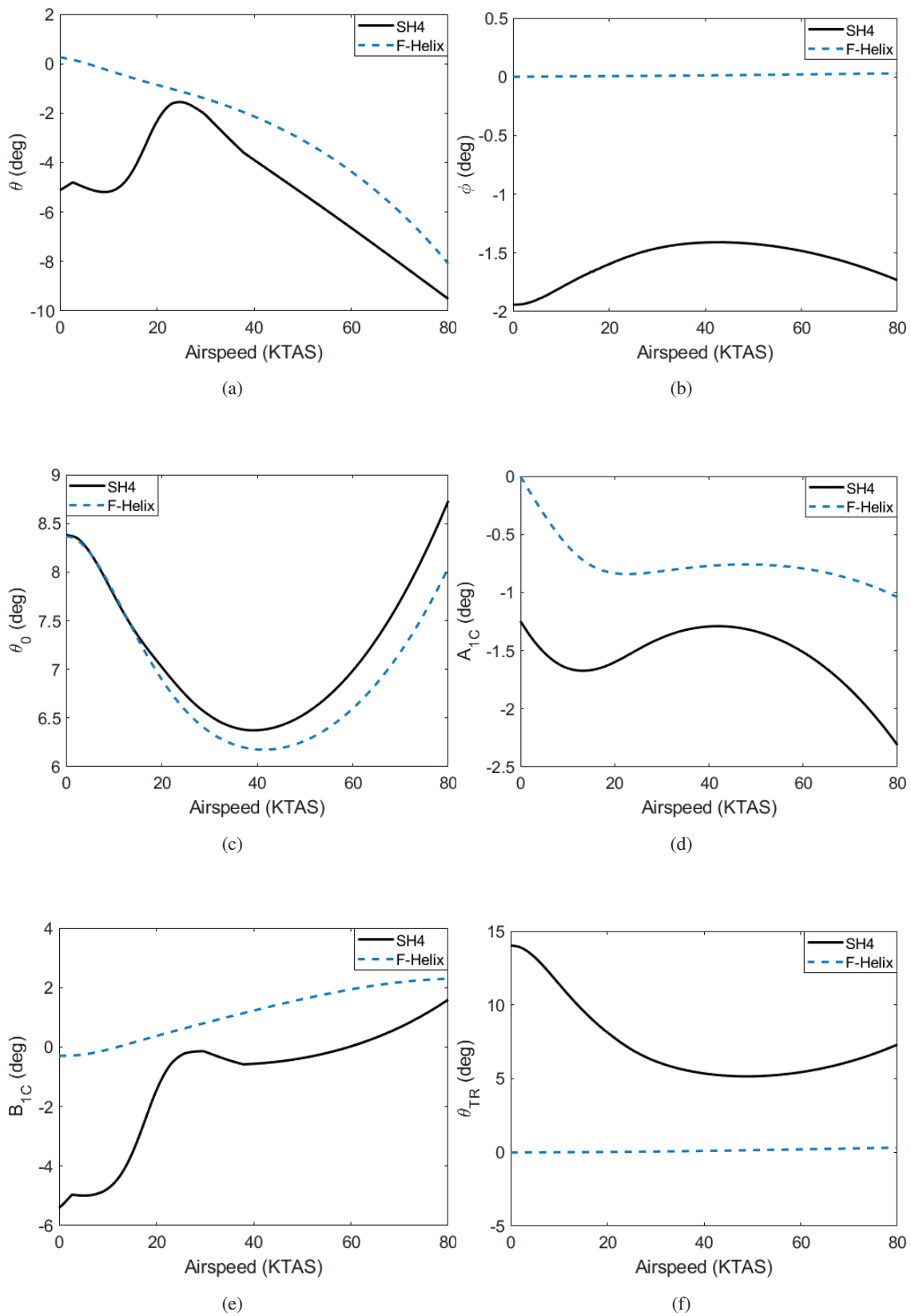


Fig. 6: Trim attitude and control commands for standard day atmospheric conditions, 1900 lbs.

reduced as explained earlier to account for the removal of the tail boom. The following figures present the point performance results for the light gross weight of 1300 lbs and the maximum takeoff gross weight of 1900 lbs. Torques are presented in torque gage units assuming that 100% torque corresponds to 170 shp at the nominal rotor rpm of 418 RPM.

Figure 7 presents the torque required to hover OGE at sea level standard atmospheric conditions. The results show that while for low weights the F-Helix requires less power to hover than the SH-4, in most gross weights the eVTOL configuration is less efficient in hover compared to the conventional rotorcraft. The gain in torque required due to the elimination of the tail rotor is the reason for the better performance of the F-Helix at very low gross weights. However, as weight is increased this gain is quickly overcome by the increased power demand of the eFans in comparison to the power required to turn the main rotor when using an internal combustion engine. At the maximum takeoff weight of 1900 lbs, the weight to power gradient of the F-Helix is 4 lbs/shp compared to the 10.7 lbs/shp of the SH-4. Figure 8 shows the power available for both configurations in various atmospheric conditions. While the performance of the internal combustion engine decreases with increasing pressure altitudes and ambient temperatures, the power output of the batteries of the eVTOL rotorcraft is approximately independent of ambient conditions, thereby largely reducing the strong dependence of hover performance on ambient conditions that is “traditional” in conventional rotorcraft. As explained earlier, for the current research it is assumed that the batteries could provide at least a maximum power output of 200 kW (158% torque gage units) and that this amount of power could be absorbed by the main rotor shaft. Figure 9 combines the information presented in Figs. 7 and 8 to present the maximum weight for hover OGE in international standard day (ISA) and international hot day (ISA+20°C) atmospheric conditions. It can be seen that the use of an electric power source weakens the effect of ambient conditions on the maximum takeoff weight. While in standard conditions the conventional rotorcraft can takeoff at the maximum allowed weight of 1900 lbs only near sea level, the eVTOL configuration extends this capability to a pressure altitude of 4000 ft. The advantage of the eVTOL configuration in terms of the maximum hover weight is even more apparent in hot day conditions where the conventional rotorcraft is limited to a maximum takeoff weight of 1780 lbs. In comparison, the eVTOL configuration maintains the capability to take off at the maximum allowed gross weight up to a pressure altitude of 1700

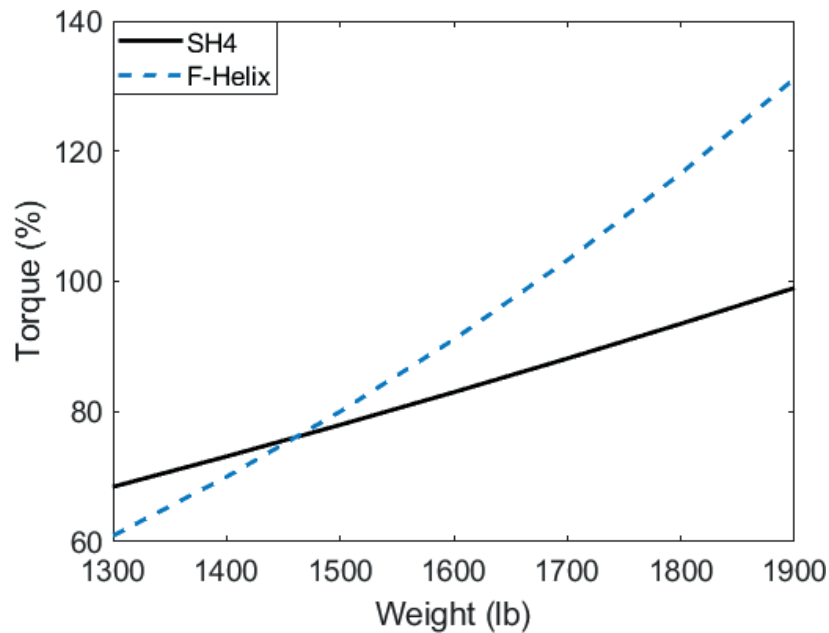


Fig. 7: Torque required for hover OGE in standard atmospheric conditions.

ft. An increase of the maximum power output limit of the batteries (which is artificially set) would increase this capability further. It can be concluded that while the aerodynamic hover performance of the eVTOL configuration is inferior to that of the conventional rotorcraft, this disadvantage is overcome by the significantly higher power output that can be obtained by using an electric power source and by the fact that this power output has practically no lapse rate with ambient atmospheric conditions. As the vehicle is intended mainly for urban air mobility in which the hover segments of the typical mission are relatively short it seems that the higher power required for hover of the eVTOL configuration is not a concern.

Figures 10 and 11 summarize the results of the forward flight performance of the F-Helix versus the SH-4. In Fig. 10 the torque required for straight and level flight are presented for both configurations for the light gross weight and maximum takeoff gross weight of 1300 lbs and 1900 lbs, respectively. It can be observed that the torque required for cruise of the eVTOL configuration is lower in significant portions of the flight envelope. The improved cruise performance of the F-Helix in these speeds is attributed mainly to the reduction in the fuselage parasite drag due to the removal of the tail boom, tail rotor and aerodynamic surfaces and the smaller pitch down trim

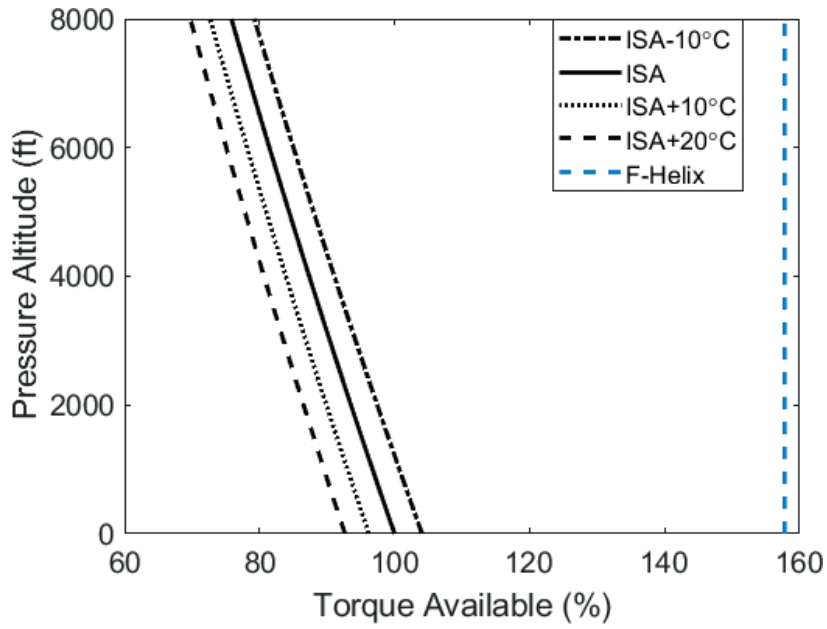


Fig. 8: Torque available for various atmospheric conditions.

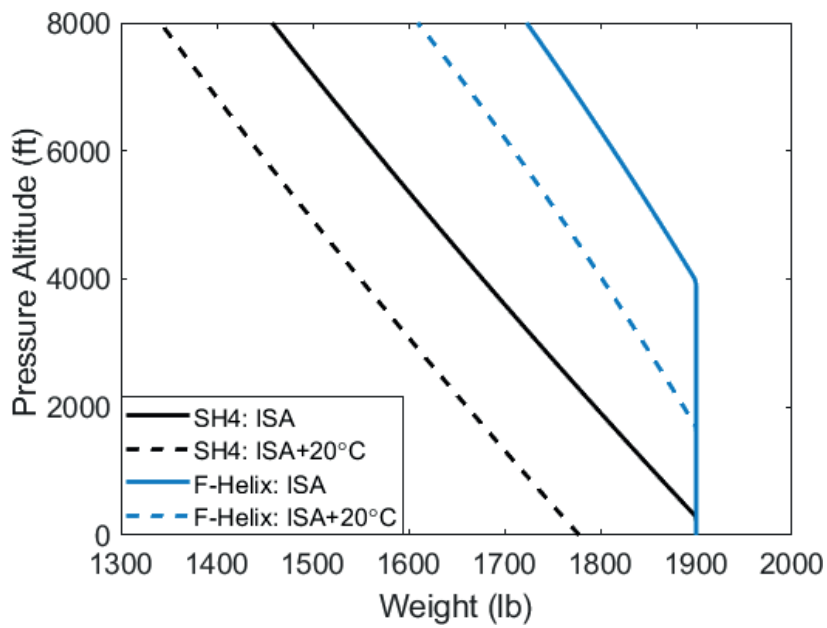


Fig. 9: Maximum hover weight OGE for standard day and hot day atmospheric conditions.



angle. At the lower and higher airspeeds the eVTOL torque required increases above that of the SH-4 due to the reduced propulsive efficiency of the eFans in comparison to that of the internal combustion engine overcoming the benefit of the reduced parasite drag of the F-Helix. The dotted lines in Fig. 10 show the optimal airspeeds for best endurance and best range for the two rotorcraft configurations. The best range speeds were determined assuming specific range values that are 99% of the maxima as this allows the increase of the best range flight speed with a minor reduction of the range performance. It can be observed that the best endurance speed of the two configurations is relatively close with the F-Helix configuration providing the best endurance at an airspeed of 42 KTAS, slightly higher than the 40 KTAS for the SH-4 configuration for the maximum takeoff weight of 1900 lbs. A much larger difference is observed for the maximum range speeds that drop by 10 KTAS from 69 KTAS for the SH-4 to 59 KTAS for the F-Helix. This is an important result as it implies an increase of 17% in the time required by the eVTOL configuration to reach a set distance relative to the conventional rotorcraft. Figure 11 presents the specific range performance for standard day conditions and a takeoff gross weight of 1900 lbs. For this analysis, two different battery types were considered for the eVTOL configuration. The first battery type assumed is a liquid Li-ion battery with a specific energy of 250 W-h/kg, which is the current state of the art for Li-ion batteries. The second battery type assumed is a solid state Li-ion battery with a specific energy of the future 625 W-h/kg. This battery type is assumed to represent the electric energy storage capabilities projected for the next decade. The results in Fig. 11 are important as they provide an estimate for the distance provided by each one pound of fuel (for the SH-4) or battery (for the F-Helix). For the conventional rotorcraft, the specific range attained at the maximum range speed is 0.91 NM/lbs. In comparison, for the eVTOL configuration with liquid Li-ion batteries at the corresponding maximum range speed this value reduces by a factor of 9 to 0.10 NM/lbs. The use of solid state batteries will provide a specific range that is 2.5 higher (0.25 NM/lbs) assuming the projected capabilities of solid state batteries materialize. However, even in this case the range performance of the eVTOL configuration will be 3.6 times lower than that of a conventional rotorcraft at the same operating weight. It follows that although the torque required for cruise by the eVTOL configuration is significantly lower than that of the conventional rotorcraft, the range obtained for each pound of battery is much lower compared to that obtained per each pound of fuel for the conventional rotorcraft. This result, a reflection of the inherently smaller energy density of electric batteries

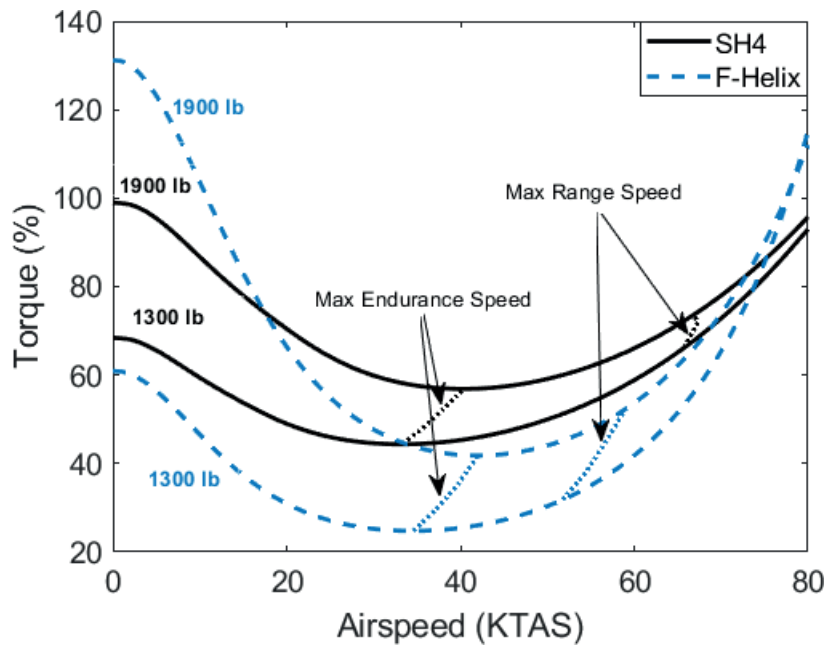


Fig. 10: Torque required for cruise in standard atmospheric conditions.

in comparison to fossil fuels is not expected to change in the near future. Therefore, in order for an eVTOL configuration to offer similar performance to that of a comparable conventional rotorcraft it should combine a more efficient cruise power with a lighter empty weight.

### C. Mission Performance

To allow the evaluation and comparison of mission performance of both configurations a typical aerial urban transportation mission is defined. The mission that is basically a one leg transport of passengers or payload is defined in a similar fashion to the preliminary mission requirements in the UBER Elevate “eVTOL Vehicle Requirements and Missions” document [10]. The segments of the urban transportation mission used for the current analysis are presented in Table IV and a graphic representation of the mission is brought in Fig. 12. The rotorcraft takes off vertically from a heliport at sea level, hovers OGE 40 feet above ground level (AGL), climbs to an altitude of 1000 ft and performs a maximum range straight and level cruise to the destination heliport. The cruise segment includes a reserve leg of 20 minutes that is not counted in the total mission time and range. The rotorcraft then descends to the destination heliport

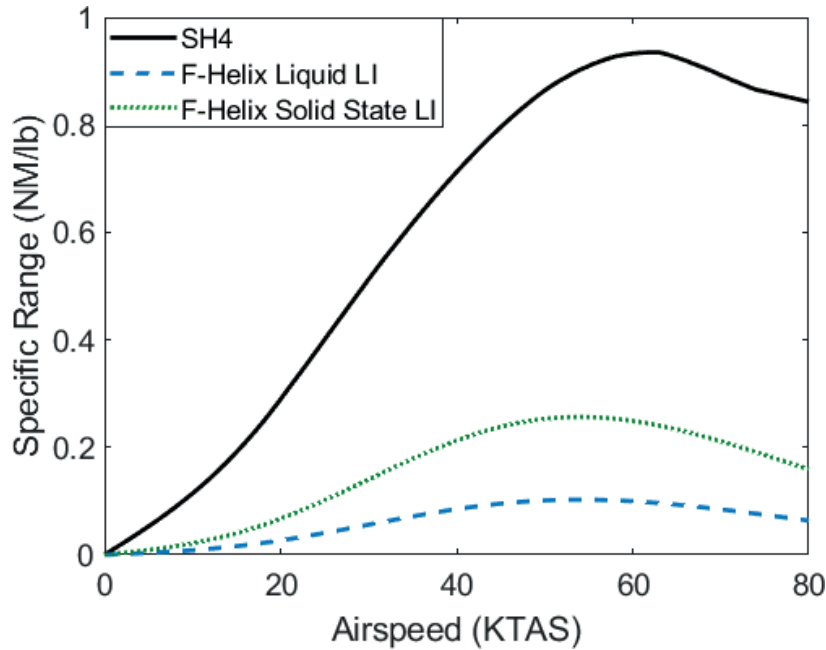


Fig. 11: Specific range in standard atmospheric conditions, 1900 lbs.

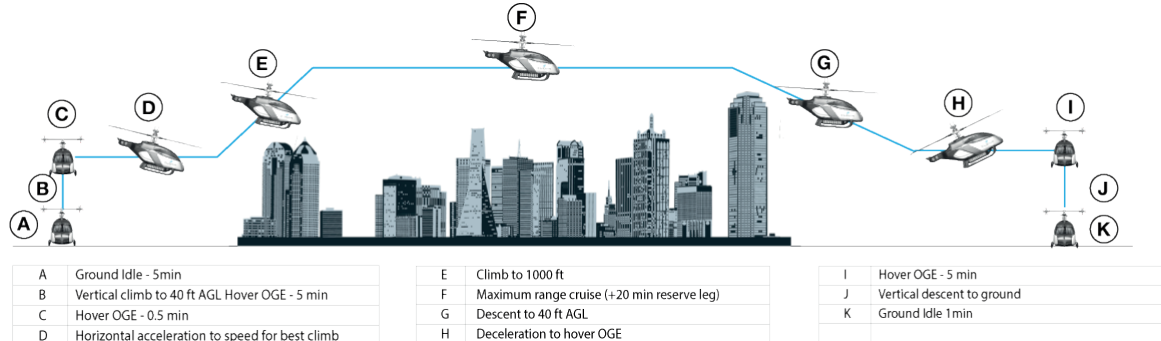


Fig. 12: Typical mission definition for payload/range performance calculation.

utilizing partial power, hovers 5 minutes OGE to simulate a situation where the heliport is busy, and lands vertically. Mission performance is calculated assuming an empty weight of 1142 lbs for the SH-4 and 650 lbs for the F-Helix for various payload weights. Since the rotorcraft is primarily intended for urban air transportation missions it is assumed that the pilot is one of the passengers and therefore is counted as “payload” in the rotorcraft configuration breakdown.

Mission performance is calculated for various payload weights. For each payload case calculated, fuel/batteries were “topped off” up to the maximum takeoff gross weight of 1900 lbs

TABLE IV: Mission Segments for Payload/Range Calculation.

Segment	Description
A	Ground Idle - 5 min
B	Vertical climb to 40 ft AGL
C	Hover OGE - 0.5 min
D	Horizontal acceleration to speed for best climb
E	Climb to 1000 ft
F	Maximum range cruise (+20 min reserve leg)
G	Descent to 40 ft AGL
H	Deceleration to hover OGE
I	Hover OGE - 5 min
J	Vertical descent to ground
K	Ground idle - 1 min

(for the SH-4 the maximum fuel quantity is limited not to exceed the fuel tank capacity of 33.5 gallons). For simplicity it is assumed that the weight of the batteries is “continuous” so that for each payload case the maximum weight margin available for battery carriage is used. Battery specific energy is then multiplied by the battery weight for the calculation of the amount of electric energy available for flight.

Figure 13 presents the results of the payload/range analysis for the typical aerial urban transportation mission defined. Results are shown for the conventional rotorcraft and for the eVTOL configuration when utilizing liquid Li-Ion batteries and solid state Li-Ion batteries. As noted above, the pilot is counted as a passenger so that the minimal payload weight in any configuration is 200 lbs, the weight of a pilot/single passenger (including baggage).

Figure 14 presents the corresponding mission times from engine startup to shutdown excluding the 20 minutes reserve leg. These figures show that the maximum range that can be attained by the SH-4 with a single passenger (pilot) is 183 NM with a corresponding mission time of 3 hours (180 min). As more passengers/payload are added the range (and corresponding flight time) is reduced. The break-point in the payload/range curve corresponds to the payload weight above

which fuel has been unloaded from the aircraft to keep the maximum takeoff gross weight limit of 1900 lbs. The conventional rotorcraft can seat one pilot and two passengers. The mission range attained in this configuration is 123 NM with a flight time of 124 min. The mission performance is significantly degraded when the conventional rotorcraft configuration is replaced by the eVTOL configuration with the liquid Li-Ion batteries. The results show that despite the reduced lower empty weight of the eVTOL rotorcraft and the lower power required for forward flight the maximum range attained with a single pilot is only 67 NM with a flight time of 81 min. Also, as shown earlier, the average flight speed is reduced from 69 KTAS with the SH-4 to 59 NM with the F-Helix so that the eVTOL rotorcraft covers less distance than the conventional rotorcraft and that the flight speed is significantly slower. The inferior mission performance of the eVTOL configuration with liquid batteries is primarily the result of the high weight of the batteries. In addition, unlike for the conventional configuration where fuel is burned during the mission thus making the rotorcraft lighter, the eVTOL configuration maintains a constant gross weight from mission start to mission end.

With the current state of the art of liquid batteries, mission performance is in line with NASA's concept vehicles for VTOL air taxi operations [11]. However, with current state of the art liquid batteries, F-Helix performance is inferior to that of the SH-4. Future solid state batteries with higher specific energy levels can provide mission performance levels that surpass those of the conventional SH-4 rotorcraft. The use of solid state batteries in place of liquid batteries with the eVTOL configuration restores the performance levels to be similar and even better than those of the conventional rotorcraft. With a single passenger (pilot), the mission range increases from 183 NM for the SH-4 to 225 with the F-Helix with solid state batteries. The corresponding flight times are 180 min and 242 min, respectively. The superior performance of the eVTOL configuration in these conditions is due to the lower empty weight of the F-Helix that allows more batteries to be added to the rotorcraft. Compared to the maximal fuel capacity of 201 lbs for the SH-4 in these conditions, the F-Helix takes off with a total battery weight of 1050 lbs. As the eVTOL gross weight remains constant at 1900 lbs throughout the mission, the range to payload gradient is constant. The lower specific range of the eVTOL configuration in comparison to the conventional configuration leads to the solid state eVTOL configuration having better mission performance than the conventional configuration, unless for payload weights between 400 lbs and 600 lbs.

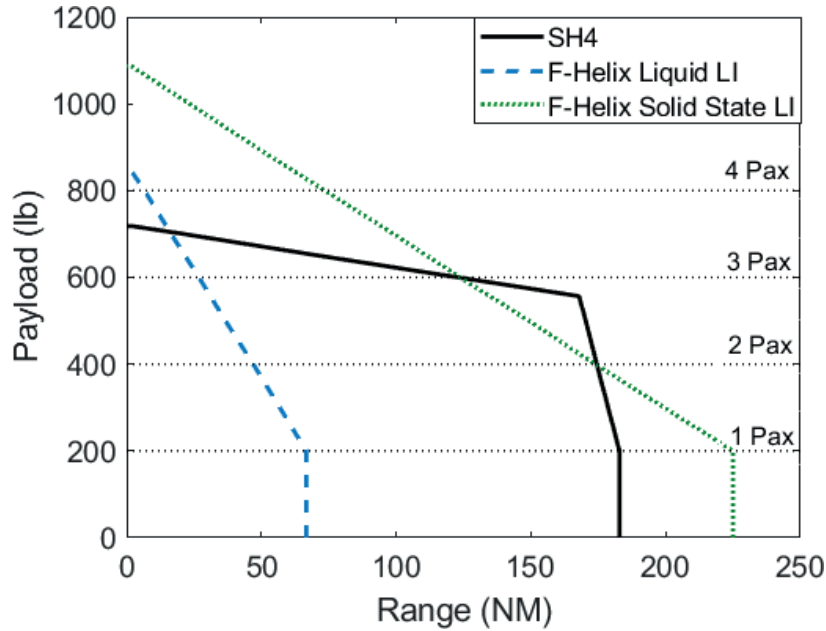


Fig. 13: Payload/range analysis results for the typical mission in standard atmospheric conditions.

This effectively means that the SH-4 has better payload/range performance only when flying with two passengers and additional payload of no more than 200 lbs. When three passengers are flown the two configurations provide the same performance with a range of 123 NM and flight times of 124 min and 139 min for the SH-4 and F-Helix configurations, respectively. With four passengers on board, the solid state F-Helix configuration will be able to fly a distance of 74 NM with a mission time of 88 min. An increase of the maximum takeoff gross weight to 2210 lbs or future batteries enabling a specific energy of more than 741 W-h/kg will make the solid state eVTOL configuration superior in terms of mission performance in any payload weight.

#### D. Autorotation Performance

The autorotation performance can be evaluated via the autorotation index, which is given by:

$$AI = \frac{I_R \Omega^2}{2W} \quad (35)$$

where  $I_R$  is the main rotor system polar moment of inertia and  $W$  is the weight of the rotorcraft. The main rotor system polar moment of inertia is given by the summation of the polar moments

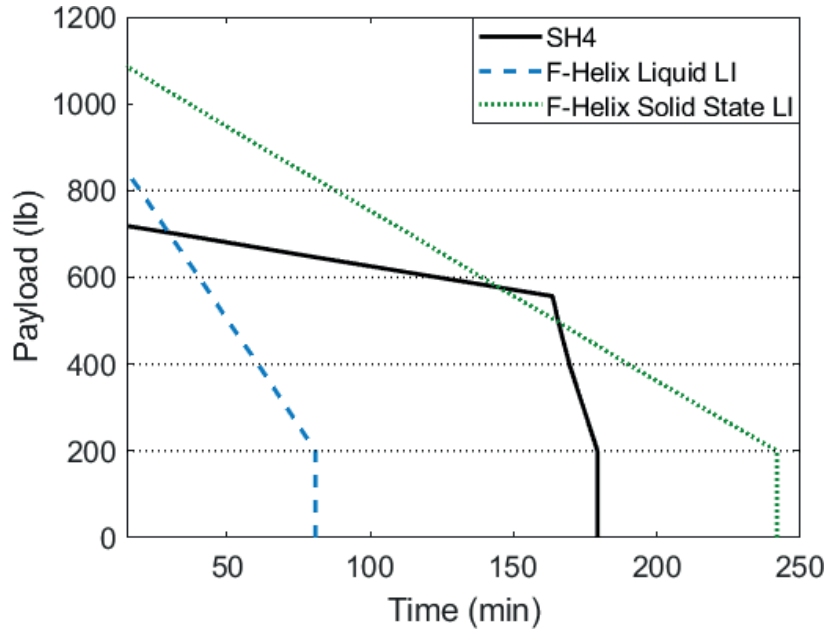


Fig. 14: Payload/mission-time results for the typical mission in standard atmospheric conditions.

of inertial of its components (i.e. blades, eFans, and power mast) with respect to the main rotor rotation axis (i.e. the axis along the main rotor shaft):

$$I_R = 2I_{\text{blade}} + I_{\text{mast}} + 2I_{\text{eFan}} \quad (36)$$

$$2I_{\text{blade}} + \frac{1}{12}m_{\text{mast}}(2r_{\text{eFan}})^2 + m_{\text{eFan}}(r_{\text{eFan}})^2 \quad (37)$$

By estimating a blade polar moment of inertia of 2740 lbs-ft<sup>2</sup> for each blade, an eFan weight of 50 lbs each, and a power mast weight of 20 lbs, the polar moment of inertia of the main rotor system is 11000 lbs-ft<sup>2</sup>. Given a maximum take-off weight of 1900 lbs, this results in an autorotation index of approximately 170. The autorotation index for the SH-4 for the same maximum take-off weight is 65. These results are compared to other helicopter's autorotation performance indices that are taken from [3], as shown in Fig. 15. Since F-Helix has a relatively high main rotor system inertia when compared to helicopters of its weight class, its autorotation index is higher than most of the helicopters shown in Fig. 15, thus leading to increased safety. Specifically, in case of loss of power, the main rotor RPM will decay more slowly than a standard

### Autorotative indices derived for several helicopters at standard sea level conditions

(data source : various published helicopters specifications)

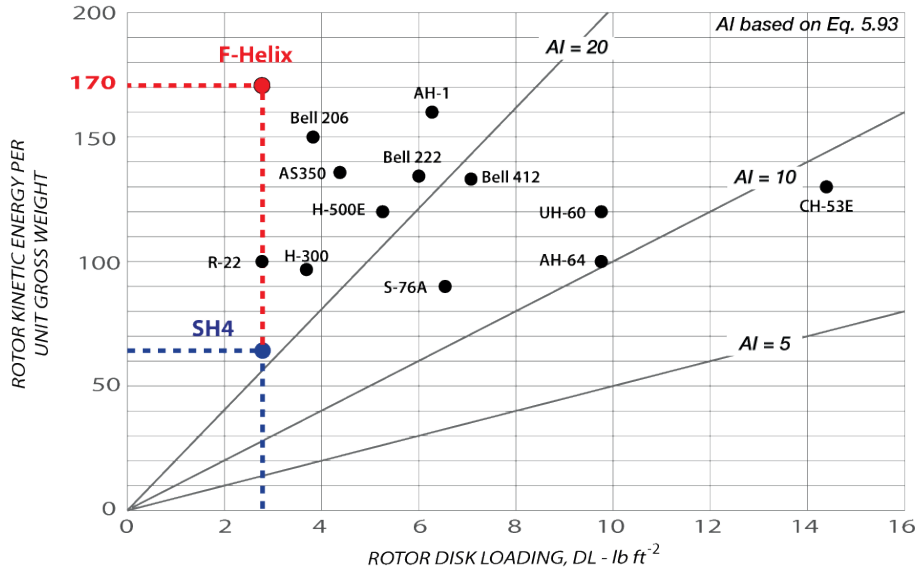


Fig. 15 : Autorotation index

helicopter, thus giving the pilot increased time to enter autorotation. Another added benefit to the F-Helix configuration is that since the rotor is not linked to an engine through a transmission, if the eFans fail, no clutch has to be disengaged between the rotor and the engine by the pilot.

## V. DYNAMIC STABILITY

Linear models are obtained by linearizing the nonlinear simulation model at incremental level flight speeds. The model is linearized at speeds from 0 to 80 kts at intervals of 10 kts. Figure 16(a) shows the eigenvalues of the 21-state model in hover, whereas Fig. 16(b) shows the eigenvalues of the 21-state model for a 80 kts level flight condition. For both conditions, the eigenvalues to the far left of the plane are relative to the inflow dynamics of the main rotor and eFans. The eigenvalues at lower frequency are relative to the rigid-body dynamics and main rotor angular dynamics, and are shown in greater detail in Fig. 17. Figure 17 shows a comparison between the 21-state and reduced-order 9-state eigenvalues. The reduced-order system eigenvalues match closely the low-frequency full-order eigenvalues. Note that for the the 80 kts case of Fig. 17(b), there is a fairly high frequency unstable eigenvalue relative to the lateral/directional dynamics, and a lower frequency unstable eigenvalue relative to the pitch/heave dynamics. This is due to the absence of a vertical and horizontal tail, respectively. A complete list of eigenvalues of

TABLE V: Reduced-order model eigenvalues in hover.

Eigenvalue	Mode	Value
$\lambda_{1,2}$	roll subsidence	$-8.3591 \pm 6.5238i$
$\lambda_3$	pitch subsidence	$-0.3389$
$\lambda_{4,5}$	pitch phugoid	$-0.2894 \pm 0.7322i$
$\lambda_6$	main rotor angular mode	$-0.0934$
$\lambda_7$	heave subsidence	$-0.0031$
$\lambda_{8,9}$	dutch roll	$0.2547 \pm 0.6455i$

the reduced-order model for both hover and forward flight is included in Tables V and VI, respectively. It is worth noting that the main rotor angular dynamics is stable.

The objective of the paper is to study the F-Helix eVTOL concept. This concept modifies the SH-4 Silvercraft light helicopter to use electric propulsion and a propeller-driven driven rotor. It is intended to compete with rotorcraft in the light-weight class and address future urban air mobility needs. The elimination of shaft driven propulsion is intended to reduce weight and drag in order to accommodate the added weight of batteries for energy storage. Once the configuration of the rotorcraft is established, the design is optimized to produce the least power required while still meeting the structural and physical constraints of its components. Next, a simulation model is developed to assess the rotorcraft performance in hover and forward flight. The payload/range performance is then evaluated for a typical aerial urban transportation mission. The performance of the eVTOL configuration is compared to the SH-4. The flight simulation model is used to assess the dynamic stability of the bare-frame aircraft, along with the stability of the main rotor system. This is done to determine whether additional aerodynamic surfaces such as horizontal and vertical stabilizers are needed to provide acceptable handling qualities to the bare-airframe. Finally, a partial authority Stability and Control Augmentation System (SCAS) is developed to give the aircraft the desired response around the roll, pitch, yaw, and heave axis. The controller also includes a main rotor RPM governor.

Given the relatively high-frequency instabilities in the lateral/directional dynamics, a vertical stabilizer is added to the F-Helix concept. The vertical tail is placed 8 ft aft of the CG (right behind the yaw fans) and has a surface area of 10 ft<sup>2</sup>. Figure 18(a) shows the eigenvalues of the 21-state model in hover, whereas Fig. 18(b) shows the eigenvalues of the 21-state model for a

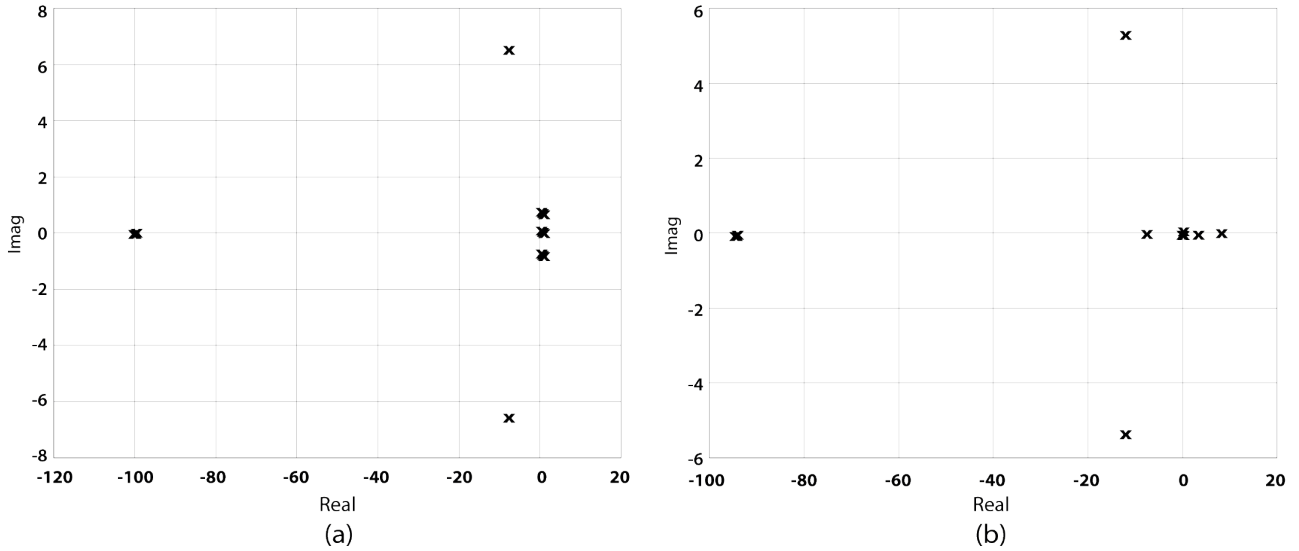


Fig. 17: Comparison between the 21-state and 9-state models eigenvalues for (a) hover and (b) 80 kts level flight.

TABLE VI: Reduced-order model eigenvalues at 80 kts level flight.

Eigenvalue	Mode	Value
$\lambda_{1,2}$	heave subsidence	$-11.9335 \pm 5.3643i$
$\lambda_3$	roll subsidence	$-7.7842$
$\lambda_{4,5}$	main rotor angular mode	$-0.3114 \pm 0.0986i$
$\lambda_6$	roll mode	$-0.0332$
$\lambda_7$	pitch phugoid	$0.2114$
$\lambda_8$	pitch subsidence	$2.7662$
$\lambda_9$	dutch roll	$7.9706$

80 kts level flight condition. For both conditions, the eigenvalues to the far left of the plane are relative to the inflow dynamics of the main rotor and eFans. The eigenvalues at lower frequency are relative to the rigid-body dynamics and main rotor angular dynamics, and are shown in greater detail in Fig. 19. Figure 19 shows a comparison between the 21-state and reduced-order

9-state eigenvalues. The reduced-order system eigenvalues match closely the low-frequency full-order eigenvalues. A complete list of eigenvalues of the reduced-order model for both hover and forward flight is included in Tables VII and VIII, respectively. It is worth noting that the main rotor angular dynamics is stable in hover and unstable with low frequency dynamics in forward flight. This will require a rotor RPM governor.

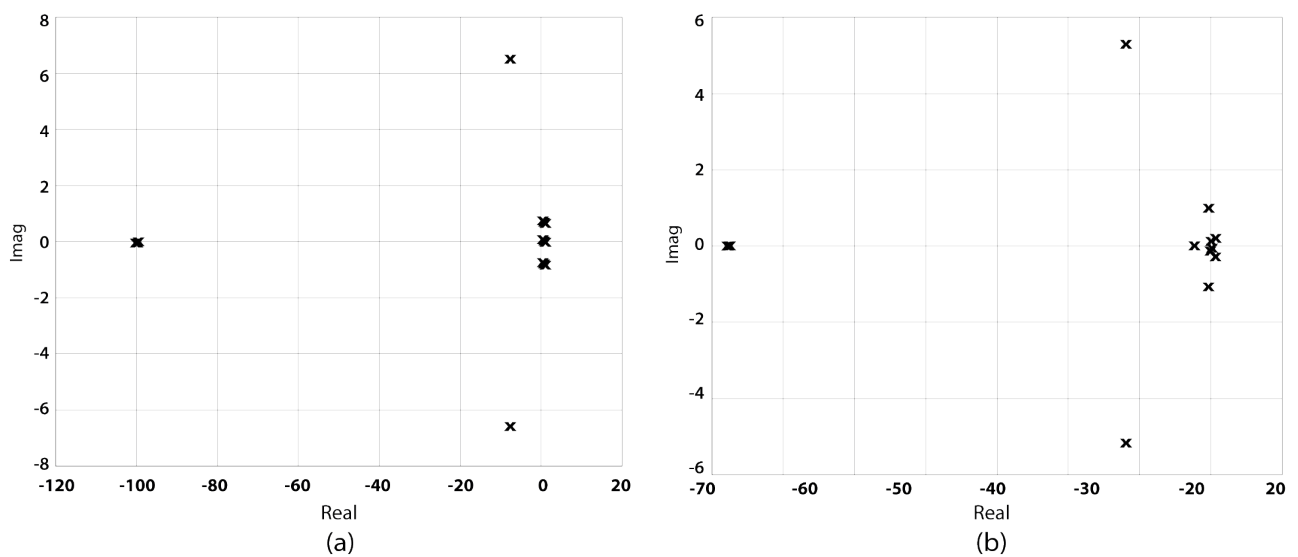


Fig. 18: Eigenvalues of the 21-state system for (a) hover and (b) 80 kts level flight (with vertical stabilizer).

## VI. FLIGHT CONTROL DESIGN

The architecture chosen for the Stability and Control Augmentation System (SCAS) is Dynamic Inversion (DI), a model-following architecture which is popular among aircraft and rotorcraft manufacturers, and in general, in the aerospace controls community. Dynamic Inversion was also used for a number of studies at Penn State over the past two decades [12], [13], [14], [15], [16]. Dynamic inversion is used to provide stability and Rate Command - Attitude Hold (RCAH) response around the roll, pitch, yaw and heave axis. Further, a DI-based governor is implemented to keep the main rotor angular speed constant.

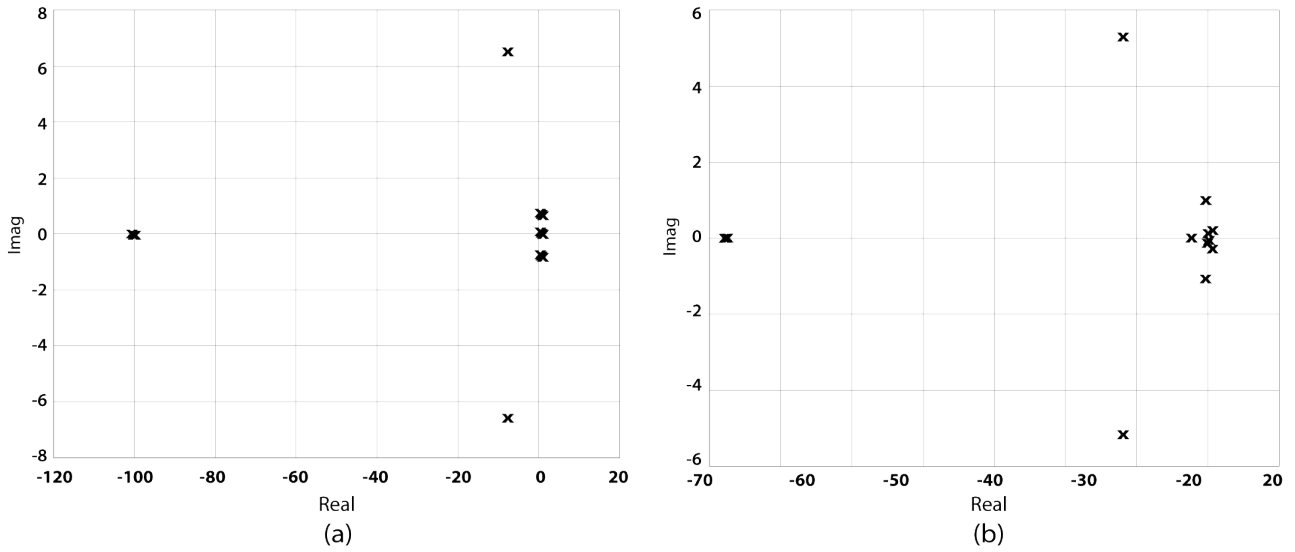


Fig. 19: Comparison between the 21-state and 9-state models eigenvalues for (a) hover and (b) 80 kts level flight (with vertical stabilizer).

TABLE VII: Reduced-order model eigenvalues in hover (with vertical stabilizer).

Eigenvalue	Mode	Value
$\lambda_{1,2}$	roll subsidence	$-8.359 \pm 6.523i$
$\lambda_3$	pitch subsidence	$-0.338$
$\lambda_{4,5}$	pitch phugoid	$-0.289 \pm 0.732i$
$\lambda_6$	main rotor angular mode	$-0.093$
$\lambda_7$	heave subsidence	$-0.003$
$\lambda_{8,9}$	dutch roll	$0.254 \pm 0.645i$

### A. Dynamic Inversion Controller

The very first step to developing a flight control law is to obtain linear models representative of the rotorcraft dynamics across the flight conditions of interest. For this reason, 21-state linear models are derived at incremental forward and level flight speeds  $V$  by means of linearization.

TABLE VIII: Reduced-order model eigenvalues at 80 kts level flight (with vertical stabilizer).

Eigenvalue	Mode	Value
$\lambda_{1,2}$	pitch subsidence	$-11.958 \pm 5.3014i$
$\lambda_3$	yaw mode	$-2.367$
$\lambda_{4,5}$	dutch roll	$-0.360 \pm 1.046i$
$\lambda_{6,7}$	pitch phugoid	$-0.293 \pm 0.346i$
$\lambda_{8,9}$	main rotor angular mode	$0.502 \pm 0.645i$

$$\dot{\mathbf{x}} = \mathbf{A}(V)\mathbf{x} + \mathbf{B}(V)\mathbf{u} \quad (38)$$

where the state and control vectors were described in the previous section. Since DI needs full-state feedback, to make the control design tractable, reduced-order models are used rather than the full-order model. The reduced-order model is obtained by means of Singular Perturbation Theory [17]. The key assumption is that the dynamics of a subset of states is substantially faster than the rest of the states. Under this condition, one can assume that the dynamics of the fast subset of states reach steady-state more quickly than the slow subset. Therefore an approximate reduced-order model that represents the slow and neglects fast phenomena of the system is derived. Specifically, the state of the 21-state models divided in slow and fast components:

$$\mathbf{x}^T = \begin{bmatrix} \mathbf{x}_s^T & \mathbf{x}_f^T \end{bmatrix} \quad (39)$$

where:

$$\hat{\mathbf{x}}_s^T = \begin{bmatrix} u & v & w & p & q & r & \phi & \theta & \Omega_{MR} \end{bmatrix} \quad (40a)$$

$$\hat{\mathbf{x}}_f^T = \begin{bmatrix} (\lambda_0 & \lambda_{1c} & \lambda_{1s})_{MR} & (\lambda_u & \lambda_l)_{eFan1} & (\lambda_u & \lambda_l)_{eFan2} \end{bmatrix} \quad (40b)$$

and the main rotor azimuth angle  $\psi_{MR}$  is truncated. The 21-state system is re-written as:

$$\begin{bmatrix} \dot{\mathbf{x}}_s \\ \dot{\mathbf{x}}_f \end{bmatrix} = \begin{bmatrix} \mathbf{A}_s & \mathbf{A}_{sf} \\ \mathbf{A}_{fs} & \mathbf{A}_f \end{bmatrix} \begin{bmatrix} \mathbf{x}_s \\ \mathbf{x}_f \end{bmatrix} + \begin{bmatrix} \mathbf{B}_s \\ \mathbf{B}_f \end{bmatrix} \mathbf{U} \quad (41)$$

Following the derivation in [18], reduced-order 9-state models are obtained:

$$\dot{\mathbf{x}}_s = \hat{\mathbf{A}}(V)\mathbf{x}_s + \hat{\mathbf{B}}(V)\mathbf{u} \quad (42)$$

where:

$$\hat{\mathbf{A}} = \mathbf{A}_s - \mathbf{A}_{sf}\mathbf{A}_f^{-1}\mathbf{A}_{fs} \quad (43a)$$

$$\hat{\mathbf{B}} = \mathbf{B}_s - \mathbf{A}_{sf}\mathbf{A}_f^{-1}\mathbf{B}_f \quad (43b)$$

Since the objective of the DI controller is to provide stability and RCAH response for the roll, pitch, yaw, heave axes, and hold the main rotor angular speed constant, the output vector is chosen to be:

$$\mathbf{y}^T = [p \ q \ r \ V_z \ \Omega_{MR}] \quad (44)$$

where  $V_z$  is the vertical speed (positive up). Define the commanded reference trajectory  $\mathbf{y}_{cmd}(t)$  as:

$$\mathbf{y}_{cmd}^T = [p_{cmd} \ q_{cmd} \ r_{cmd} \ V_{zcmd}] \quad (45)$$

The output matrix that relates the state vector with the output vector (or controlled variables) is scheduled with speed and is given by:

$$\mathbf{C}(V) = \begin{bmatrix} 0 & 0 & 0 & 1 & 0 & 0 & 0 & 0 & 0 \\ 0 & 0 & 0 & 0 & 1 & 0 & 0 & 0 & 0 \\ 0 & 0 & 0 & 0 & 0 & 1 & 0 & 0 & 0 \\ 0 & 0 & -1 & 0 & 0 & 0 & 0 & V & 0 \\ 0 & 0 & 0 & 0 & 0 & 0 & 0 & 0 & 1 \end{bmatrix} \quad (46)$$

The DI control law is given by:

$$\mathbf{u} = (\mathbf{C}\hat{\mathbf{B}})^{-1}(\nu - \mathbf{C}\hat{\mathbf{A}}\mathbf{x}_s) \quad (47)$$

where  $\nu$  is the pseudo-command vector and  $\mathbf{e}$  is the error as given respectively in Eq. 48 and Eq. 49.



$$\begin{bmatrix} \nu_p \\ \nu_q \\ \nu_r \\ \nu_{V_z} \\ \nu_{\Omega_{MR}} \end{bmatrix} = \begin{bmatrix} \ddot{p}_{cmd} \\ \ddot{q}_{cmd} \\ \dot{r}_{cmd} \\ \dot{V}_{zcmd} \\ \dot{\Omega}_{MRcmd} \end{bmatrix} + \mathbf{K}_P \begin{bmatrix} e_p \\ e_q \\ e_r \\ e_{V_z} \\ e_{\Omega_{MR}} \end{bmatrix} + \mathbf{K}_I \begin{bmatrix} \int e_p dt \\ \int e_q dt \\ \int e_r dt \\ \int e_{V_z} dt \\ \int e_{\Omega_{MR}} dt \end{bmatrix} \quad (48)$$

$$\mathbf{e} = \mathbf{y}_{cmd} - \mathbf{y}; \quad (49)$$

The 5-by-5 diagonal matrices  $\mathbf{K}_P$  and  $\mathbf{K}_I$  identify the proportional and integral gain matrices, respectively.

### B. Error Dynamics

Feedback compensation is needed to ensure the system tracks the command models. It can be demonstrated [19] that for a Dynamic Inversion controller the output equation must be differentiated  $n$  times for the controls to appear explicitly in the output equation:

$$e^{(n)} = \nu - y_{cmd}^{(n)} \quad (50)$$

Since in the present case the output equation has to be derived only one time for the controls to appear explicitly in the output equation, a Proportional-Integral (PI) control strategy is applied to the pseudo-command vector:

$$\nu = \dot{y}_{cmd}(t) + K_P e(t) + K_I \int_0^t e(\tau) d\tau \quad (51)$$

By substituting Eq. 51 into Eq. 50, the closed-loop error dynamics is obtained:

$$\dot{e}(t) + K_P e(t) + K_I \int_0^t e(\tau) d\tau = 0 \quad (52)$$

The gains can be chosen so that the frequencies of the error dynamics are of the same order as the command filters (i.e. first order), ensuring that the bandwidth of the response to disturbances is comparable to the one of an input given by a pilot or outer loop. By taking the Laplace transform, and therefore switching to the frequency domain, the error dynamics becomes:

$$e(s) (s^2 + sK_P + K_I) = 0 \quad (53)$$

In order to obtain the gains that would guarantee a desired response, the error dynamics can be set equal to a second-order system given in Eq. 54:

$$s^2 + 2\zeta\omega_n s + \omega_n^2 = 0 \quad (54)$$

Setting the coefficients of the polynomial equal to the the gains of Eq. 53 results in:

$$K_P = 2\zeta\omega_n \quad (55a)$$

$$K_I = \omega_n^2 \quad (55b)$$

## VII. BATCH SIMULATIONS

The Dynamic Inversion flight controller is tested in batch simulations. The flight condition in consideration is 65 kts level flight. Figure 20 shows how the closed-loop system is able to track the commanded pitch rate following a longitudinal stick doublet. Figure 21 shows the attitude response to a longitudinal stick doubled. It is worth noting that the off-axis response is very well-contained. Figure 22 shows the eFan inflow response to a longitudinal stick doublet. It is worth noting that the amplitude of oscillation of the inflow ratio for the eFan upper (or front) rotors is substantially higher than the eFan lower (or aft) rotors. This suggests that the upper (or front) rotor of each eFan acts as a filter for inflow of the lower (or aft) rotor. This is an interesting result coming out of this analysis. Lastly, Fig. 23 shows how the main rotor angular speed is kept approximately constant, or anyways stable, by the main rotor RPM governor. Although results for the other axes that the SCAS acts on are omitted for the sake of brevity, it is concluded that the Dynamic Inversion flight controller stabilizes the aircraft and provides rate command / attitude hold response on the roll, pitch, yaw, heave, and main rotor angular speed axes.

## VIII. CONCLUSION

First, the validity of the initial concept was assessed. Once the configuration of the rotorcraft was established, the design was optimized to produce the least power required while still meeting the structural and physical constraints of its components. Next, a simulation model was developed to assess the performances in hover and forward flight. The payload/range performance was then evaluated for a typical aerial urban transportation mission. The performance of the eVTOL configuration was compared to the SH-4. The flight simulation model was used to assess the dynamic stability of the bare-frame aircraft, along with the stability of the main rotor system.

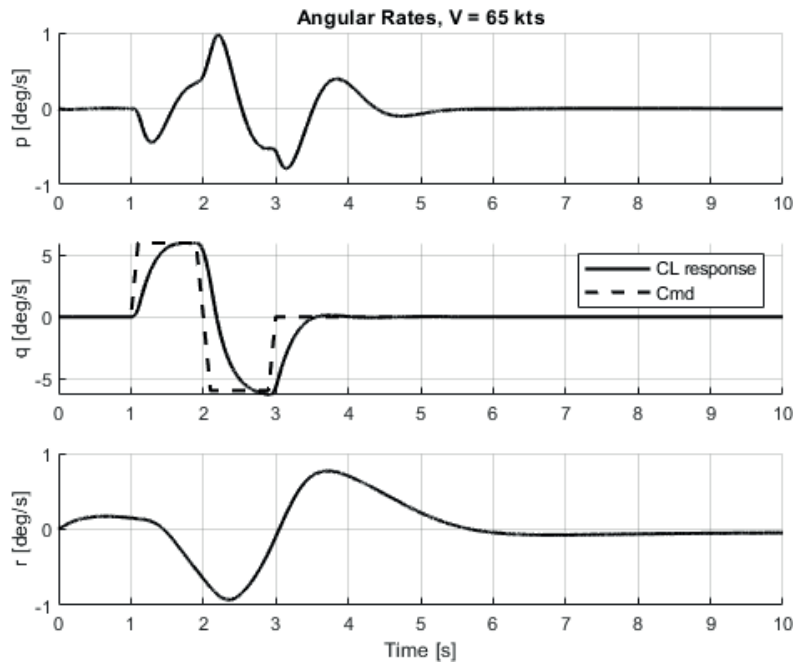


Fig. 20: Angular rates response to a longitudinal stick doublet at 65 kts level flight.

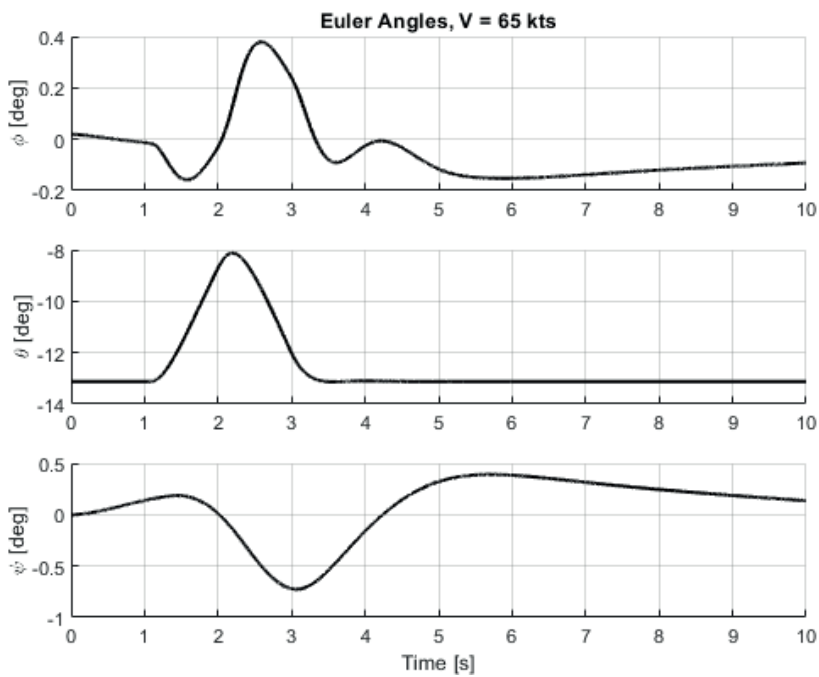


Fig. 21: Attitude response to a longitudinal stick doublet at 65 kts level flight.

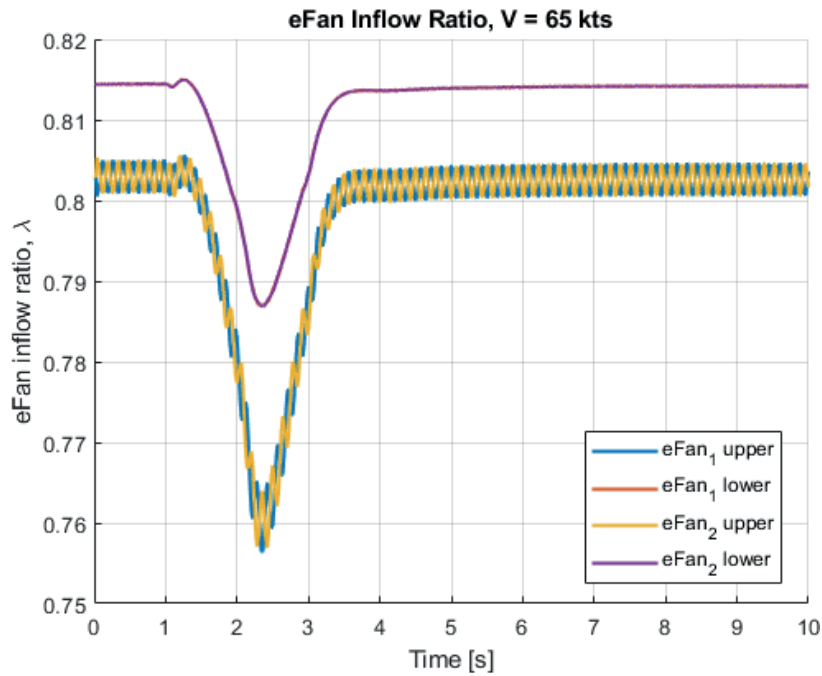


Fig. 22: eFan inflow ratio response to a longitudinal stick doublet at 65 kts level flight.

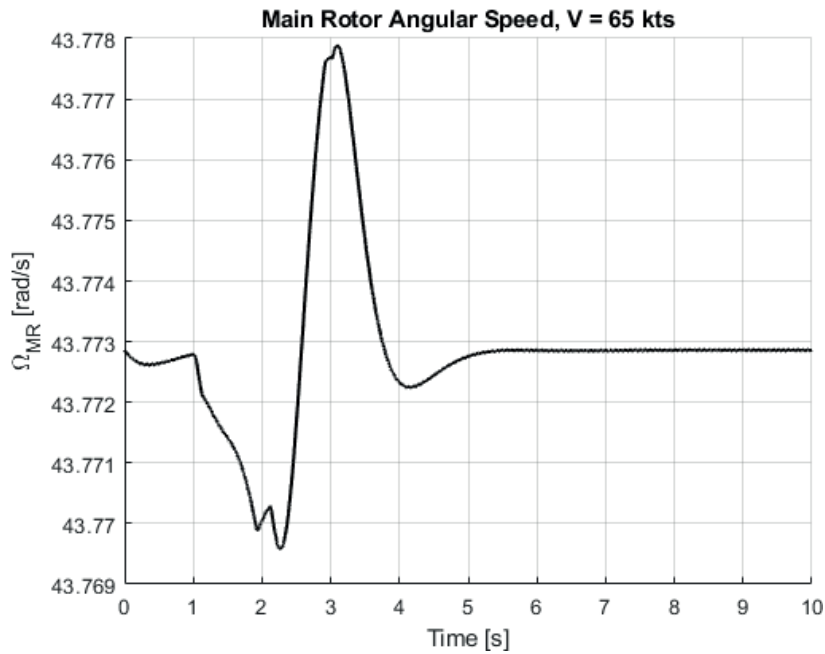


Fig. 23: Main rotor system angular speed response to a longitudinal stick doublet at 65 kts level flight.



Finally, a partial authority Stability and Control Augmentation System (SCAS) was developed to provide the aircraft with stability and desired response around the roll, pitch, yaw, and heave axis. The controller also includes a main rotor RPM governor. Based on this work, the following conclusions are drawn.

- 1) Because of the high centrifugal loads the eFans are subjects to, they are moved inboard with respect to the initial configuration. Since the structural integrity of the nacelles of possibly ducted eFans is a matter of concern under high centrifugal loads, unducted propellers chosen in favor of ducted fans.
- 2) Since the eFans spin in a rotating frame, they are subject to high gyroscopic moments. It is decided to mount two counter-rotating coaxial propellers per eFan, so that the overall gyroscopic moment is zero.
- 3) To control the yaw axis, it is chosen to use two counter-rotating fixed-pitch ducted fans that provide thrust in each directions. This is eliminates possible delays in control action that a single tail rotor would give if it had to reverse the direction of its thrust vector.
- 4) The F-Helix eVTOL configuration allows trimmed flight with near-zero fuselage roll angles and improves the apparent longitudinal stability of the rotorcraft.
- 5) F-Helix power required to hover at maximum takeoff weight (1900 lbs) is higher than that of the conventional SH-4 rotorcraft due to the reduced propulsive efficiency of the eFans in comparison to that of an internal combustion engine. However, hover performance of the F-Helix is superior due to the higher power available by the batteries and the independence of this power output on ambient atmospheric conditions.
- 6) The elimination of the need for an anti-torque system for the eVTOL configuration and the resulting exclusion of the tail rotor, tail boom, and aerodynamic surfaces reduces the power required for cruise in comparison to the conventional rotorcraft for large parts of the flight envelope. Best-endurance speeds for the eVTOL configurations are similar to those of the original SH-4 but best-range speeds are reduced by 10 KTAS. The F-Helix is thus expected to be slower in maximum range cruise missions.
- 7) The specific range of the eVTOL configuration is significantly lower than that of the conventional configuration due to the inherent lower energy density of electric batteries in comparison to fossil fuels. Therefore, in order for an eVTOL configuration to offer

similar performance to that of a comparable conventional rotorcraft, it should combine a more efficient cruise power with a lighter empty weight.

- 8) With the current state of the art of liquid batteries, mission performance is in line with, if not superior to, NASA's concept vehicles for VTOL air taxi operations. However, with current state of the art liquid batteries, F-Helix performance is inferior to that of the SH-4. Future solid state batteries with higher specific energy levels can provide mission performance levels that surpass those of the conventional SH-4 rotorcraft.
- 9) A vertical tail was added due to a high-frequency instability in the lateral/directional dynamics in forward flight. The vertical stabilizer effectively brings the center of pressure closer to the CG, thus diminishing the frequency of the instability and making it manageable for the controller to stabilize the aircraft.
- 10) The main rotor angular dynamics is stable in hover and unstable with low-frequency dynamics in forward flight. A main rotor RPM governor is implemented as a consequence of this.
- 11) A Dynamic Inversion-based partial authority Stability and Control Augmentation System (SCAS) was developed to provide the aircraft with stability and desired response around the roll, pitch, yaw, and heave axis.

## REFERENCES

- [1] Online, [www.f-helix.com](http://www.f-helix.com).
- [2] Online, [www.siemens.com/press/en/feature/2015/corporate/2015-03-electromotor.php?content\[\]=Corp](http://www.siemens.com/press/en/feature/2015/corporate/2015-03-electromotor.php?content[]=Corp).
- [3] Leishman, J. G., *Principles of Helicopter Aerodynamics*, Cambridge University Press, New York, New York, 2006.
- [4] Anon, *Aeronautical Design Standard Performance Specification, Handling Qualities Requirements for Military Rotorcraft*, ADS-33-PRF, USAAMCOM, 2000.
- [5] Pitt, D. M., and Peters, D. A., *Theoretical prediction of dynamic-inflow derivatives*, Vertica, Vol. 5, (1), March, 1981, pp. 21-34.
- [6] Anon, *Specific Airworthiness Specification SilverCraft SH-4*, EASA.SAS.R.001, May 2, 2011.
- [7] Taylor, J. W. R., ed. *Jane's All The World's Aircraft 1976-77*, Franklin Watts, 1976.
- [8] Howlett, J. J., *UH-60A Black Hawk Engineering Simulation Program: Volume I - Mathematical Model*, SER 70452 (NASA Contractor Report 166309), December, 1981.
- [9] O, HO, IO, AIO, HIO, TIO-360 Series Operator's Manual, Lycoming Part Number: 60297-12, Revision no. 60297-12-5, June, 2007.



- [10] Anon, *eVTOL Vehicle Requirements and Missions*, UBER Elevate, June 6, 2018. Online, <https://s3.amazonaws.com/uber-static/elevate/Summary+Mission+and+Requirements.pdf>
- [11] Johnson, W., Silva, C., and Solis, E., *Concept Vehicles for VTOL Air Taxi Operations*, AHS Technical Conference on Aeromechanics Design for Transformative Vertical Flight, San Francisco, CA, January 16-19, 2018
- [12] Horn, J. F., *Non-Linear Dynamic Inversion Control Design for Rotorcraft*, Aerospace 2019, 6, 38.
- [13] Saetti, U., J., Horn, J. F., Lakhmani, S., Lagoa, C., and Berger, T., *Design of Dynamic Inversion and Explicit Model Following Control Laws for Quadrotor Inner and Outer Loops*, Vertical Flight Society 74th Annual Forum Proceedings, Phoenix, AZ, May 14-17, 2018.
- [14] Saetti, U. Horn, J. F., Villafana, W., Sharma, K., and Brentner, K. S., *Rotorcraft Simulations with Coupled Flight Dynamics, Free Wake, and Acoustics*, American Helicopter Society 72th Annual Forum Proceedings, West Palm Beach, FL, May 16-19, 2016.
- [15] Caudle, D. B., *DAMAGE MITIGATION FOR ROTORCRAFT THROUGH LOAD ALLEVIATING CONTROL*, M.S. Thesis, The Pennsylvania State University, December 2014.
- [16] Spires, J. M., and Horn, J. F. *Multi-Input Multi-Output Model-Following Control Design Methods for Rotorcraft*, AHS 71<sup>st</sup> Annual Forum, Virginia Beach, VA, May 5-7, 2015.
- [17] Kokotovic, P. V., O'Malley, R. E., and Sannuti, P., *Singular Perturbations and Order Reduction in Control Theory, an Overview*, Automatica, Vol. 12, (2), 1976, pp. 123-132.
- [18] Saetti, U., and Horn, J. F., *Use of Harmonic Decomposition Models in Rotorcraft Flight Control Design with Alleviation of Vibratory Loads*, 43rd European Rotorcraft Forum, Milan, Italy, September 2017.
- [19] Stevens, B. L., and Lewis, F. L., *Aircraft Control and Simulation: Dynamics, Controls Design, and Autonomous Systems, Third Edition*, John Wiley and Sons, Inc., New York, October 2015.